Cell Reports

Article

Selective induction of human renal interstitial progenitor-like cell lineages from iPSCs reveals development of mesangial and EPO-producing cells

Graphical abstract

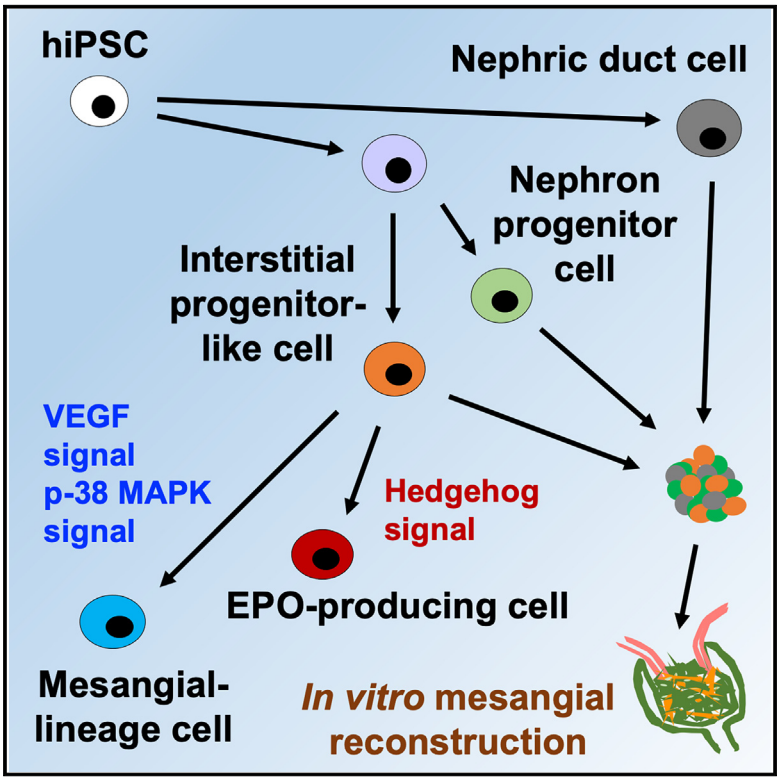

Highlights

- A selective induction method for renal IPC-like cells from hiPSCs was established
- Co-culture of hiPSC-derived IPLCs and NPCs form mesangium-like structures *in vitro*
- hiPSC-derived IPLCs develop mesangial and EPO-producing cell lineages *in vitro*
- Crucial roles of p38 MAPK signaling in mesangial-lineage development were revealed

Authors

Hiraku Tsujimoto, Azusa Hoshina, Shin-Ichi Mae, ..., Cecilia Graneli, Kevin J. Woollard, Kenji Osafune

Correspondence

osafu@cira.kyoto-u.ac.jp

In brief

Tsujimoto et al. establish the selective induction of renal interstitial progenitor-like cells (IPLCs) from hiPSCs. These IPLCs form mesangium-like structures when combined with hiPSC-derived nephron progenitor cells and selectively differentiate into mesangial and EPO-producing cells *in vitro*, revealing crucial roles of p38 MAPK, VEGF, and hedgehog signaling in interstitial development.

Tsujimoto et al., 2023, Cell Reports *43*, 113602
February 27, 2023
https://doi.org/10.1016/j.celrep.2023.113602

CellPress

Cell Reports

CellPress
OPEN ACCESS

Article

Selective induction of human renal interstitial progenitor-like cell lineages from iPSCs reveals development of mesangial and EPO-producing cells

Hiraku Tsujimoto,[1,2] Azusa Hoshina,[1] Shin-Ichi Mae,[1] Toshikazu Araoka,[1] Wang Changting,[1] Yoshihiro Ijiri,[1] May Nakajima-Koyama,[1] Satoko Sakurai,[1] Kazusa Okita,[1] Ken Mizuta,[3] Akira Niwa,[1] Megumu K. Saito,[1] Mitinori Saitou,[1,3,4] Takuya Yamamoto,[1,4,5] Cecilia Graneli,[6] Kevin J. Woollard,[7] and Kenji Osafune[1,8,*]

[1]Center for iPS Cell Research and Application (CiRA), Kyoto University, 53 Kawahara-cho, Shogoin, Sakyo-ku, Kyoto 606-8507, Japan
[2]Rege Nephro Co., Ltd., Med-Pharm Collaboration Building, Kyoto University, 46-29 Yoshidashimoadachi-cho, Sakyo-ku, Kyoto 606-8501, Japan
[3]Department of Anatomy and Cell Biology, Graduate School of Medicine, Kyoto University, Kyoto 606-8501, Japan
[4]Institute for the Advanced Study of Human Biology (WPI-ASHBi), Kyoto University, Kyoto 606-8501, Japan
[5]Medical-risk Avoidance based on iPS Cells Team, RIKEN Center for Advanced Intelligence Project (AIP), Kyoto 606-8507, Japan
[6]BioPharmaceuticals R&D Cell Therapy, Research and Early Development, Cardiovascular, Renal and Metabolic (CVRM), BioPharmaceuticals R&D, AstraZeneca, 431 83 Gothenburg, Sweden
[7]Bioscience Renal, Research and Early Development, Cardiovascular, Renal and Metabolic, BioPharmaceuticals R&D, AstraZeneca, Cambridge CB2 0AA, UK
[8]Lead contact
*Correspondence: osafu@cira.kyoto-u.ac.jp
https://doi.org/10.1016/j.celrep.2023.113602

SUMMARY

Recent regenerative studies using human pluripotent stem cells (hPSCs) have developed multiple kidney-lineage cells and organoids. However, to further form functional segments of the kidney, interactions of epithelial and interstitial cells are required. Here we describe a selective differentiation of renal interstitial progenitor-like cells (IPLCs) from human induced pluripotent stem cells (hiPSCs) by modifying our previous induction method for nephron progenitor cells (NPCs) and analyzing mouse embryonic interstitial progenitor cell (IPC) development. Our IPLCs combined with hiPSC-derived NPCs and nephric duct cells form nephrogenic niche- and mesangium-like structures *in vitro*. Furthermore, we successfully induce hiPSC-derived IPLCs to differentiate into mesangial and erythropoietin-producing cell lineages *in vitro* by screening differentiation-inducing factors and confirm that p38 MAPK, hypoxia, and VEGF signaling pathways are involved in the differentiation of mesangial-lineage cells. These findings indicate that our IPC-lineage induction method contributes to kidney regeneration and developmental research.

INTRODUCTION

Metanephros, the kidney primordium in amniotes, is formed from at least three essential types of progenitor cells derived from an early embryonic germ layer, the intermediate mesoderm (IM): nephron progenitor cells (NPCs), which give rise to epithelia of glomeruli and renal tubules; ureteric bud (UB) cells, which differentiate into the epithelia of collecting ducts and lower urinary tract; and interstitial progenitor cells (IPCs).[1,2] A fate-mapping study showed that the developmental origins at embryonic day 10.5 (E10.5) of renal epithelial and interstitial cells are different. Cells labeled with neither the NPC marker Six2[3] nor HoxB7 using its promoter specifically within the nephric duct (ND) lineages[4] contributed to interstitial cells, but cells labeled with the IPC marker Foxd1 gave rise to interstitial cells.[5] Other studies showed that IPCs can arise from common progenitor cells with NPCs at E9.5, while cells positive for an IM marker, Osr1, between E9.5 and E10.5, Osr1(−) cells at E11.5, and Foxd1(+) cells after E10.5 give rise to only IPCs.[6–9] Signals from interstitial cells are essential for forming the complex dendritic-like structures of the kidney, especially those of the collecting ducts.[10] IPCs give rise to not only diverse stroma[11] but also mesangial cells and vascular pericytes.[5] Other reports suggested that erythropoietin (Epo) production first occurs in neural crest or neuroepithelium and then in liver but at around birth, the kidneys take over production.[12] Epo-producing cells in kidney are considered a derivative of Foxd1(+) IPCs.[13] IPC lineages are also useful in models for kidney diseases. For example, renal interstitium is the primary site of kidney fibrosis, and mesangium plays important roles in glomerular function and pathology.[5,14]

Several groups have generated multi-lineage kidney organoids containing interstitial cells by manipulating the interaction of anterior and posterior IM differentiated from human pluripotent stem cells (hPSCs).[15,16] A recent study generated IPCs from mouse embryonic stem cell (ESC)-derived ROBO2(+) PDGFRA(+)-sorted mesodermal cells after treatment with

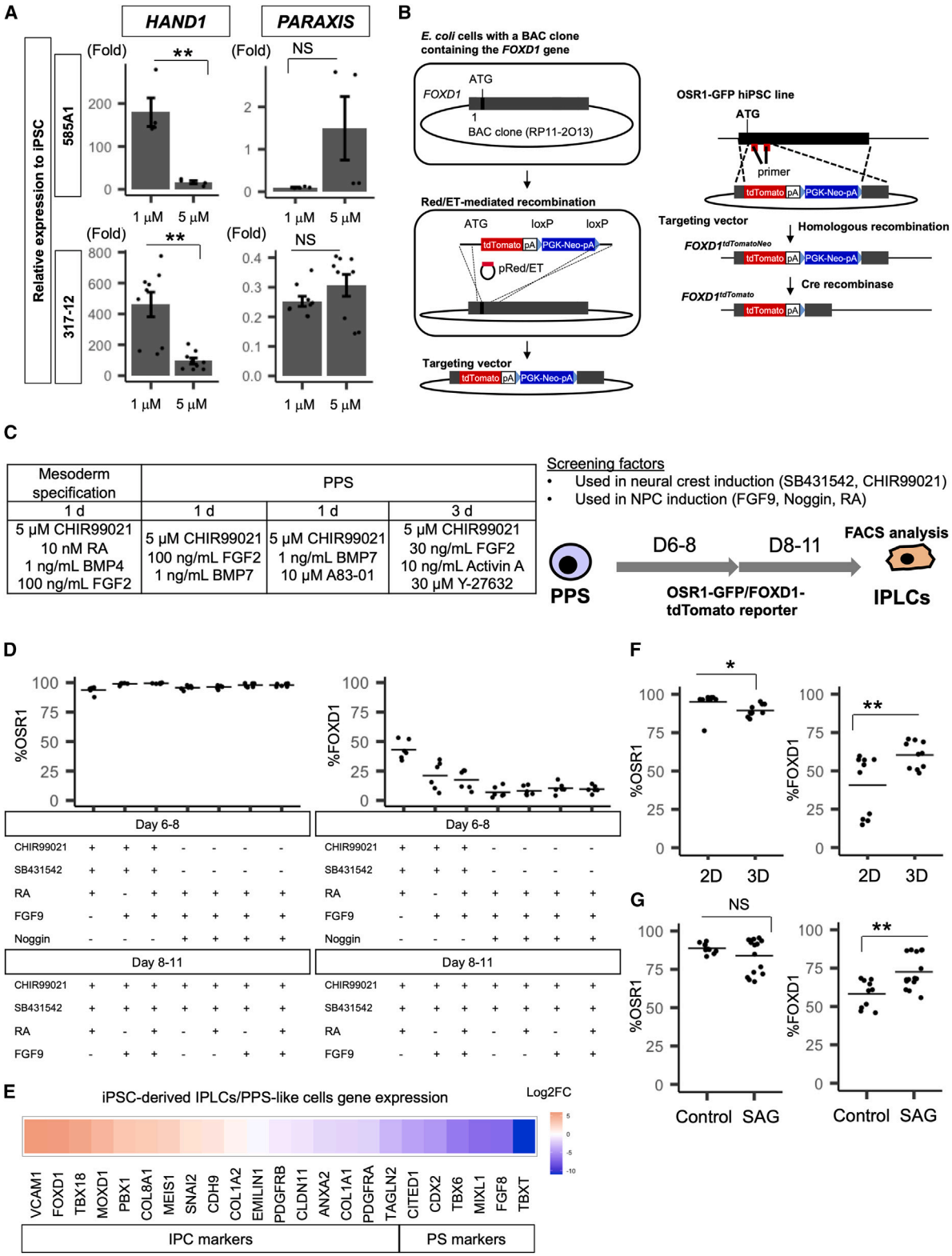

Figure 1. Induction of renal IPLCs from hiPSCs

(A) RT-qPCR analysis of *HAND1* and *PARAXIS*. The values were normalized to that of undifferentiated hiPSCs. Data are presented as the mean ± SEM, and dots indicate independent experimental data using 585A1 cells (n = 4) and 317-12 cells (n = 9).

(legend continued on next page)

fibroblast growth factor 9 (FGF9), retinoic acid (RA), the bone morphogenetic protein (BMP) inhibitor LDN-193189, sonic hedgehog (SHH), and Y-27632.[8] However, the selective induction of renal IPCs from hPSCs has not been achieved.

In this study, we first modified the posterior mesodermal progenitor cell induction step of our previously reported NPC differentiation protocol from human induced pluripotent stem cells (hiPSCs) and developed a method to selectively induce interstitial progenitor-like cells (IPLCs). The induced IPLCs were used to elucidate the developmental mechanisms of IPC-derived cells including mesangial and EPO-producing cell lineages.

RESULTS

Robust induction of metanephric mesenchyme-committed posterior primitive streak and NPCs from hiPSCs

We previously reported an induction method to generate posterior primitive streak (PPS)-like cells from hiPSCs under a 2D culture using Matrigel-coated plates.[17] In this study, we found that using a higher concentration (5 μM) of the GSK-3β inhibitor CHIR99021 on culture days 0–1 more efficiently induced PPS-like cells on day 6 that weakly express a lateral plate mesoderm marker, *HAND1*, compared with our original protocol using 1 μM CHIR99021 (Figure 1A). Different hiPSC lines showed different optimal CHIR99021 treatment durations[18] and different endogenous expression levels of BMPs.[19] Consistently, we found different expression levels of the paraxial mesodermal marker *PARAXIS*, *OSR1*, and the PPS marker *HOXA11* between two hiPSC lines on day 6 by the same treatment (Figures 1A and S1A). However, immunostaining and gene expression analyses on day 6 showed expressions of the primitive streak (PS) markers T and TBX6 were maintained regardless of the CHIR99021 concentration, indicating that the two culture conditions both generate PPS (Figures S1A and S1B). A temporal analysis of cell density during the differentiation of NPCs from PPS using this modified method revealed that the cells became too dense, resulting in cell aggregates and the unstable induction of NPCs. Therefore, we reseeded the cells on day 4 using a laminin-premixed method[20] and confirmed that the cells spread evenly.

Laminin isoforms have been optimized to coat cell-culture plates.[21] Accordingly, we examined the effects of laminin coating but found the induction efficiency of OSR1(+) cells on day 11 was higher in cultures without matrices upon day-4 reseeding, which generated partially attached cell aggregates. Therefore, we tested a complete floating and agitated culture condition on days 4–11 in a stirred bioreactor and evaluated the induction rate of OSR1(+)SIX2(+) cells by comparing four groups: no reseeding, reseeding on day 4 and 2D culture with or without matrix and reseeding on day 4, and agitated culture (Figure S1C and Item S1 tab S1C). Reseeding improved the OSR1(+)SIX2(+) cell rate on day 11 compared with no reseeding, but reseeding with the agitated culture tended to have the biggest effect (around 80%; Figures S1C and S1D). Immunostaining day-6 reseeded cells with 3D culture for two PPS markers (CITED1 and HOXC1) also showed an induction efficiency of PPS cells at around 80% (Figure S1E). Overall, these data indicate that switching from 2D to 3D culture efficiently induces metanephric mesenchyme (MM)-committed PPS cells and improves the induction efficiency of OSR1(+)SIX2(+) NPCs (Figure S1F).

Induction of FOXD1(+) IPLCs from PPS

To quantitatively evaluate the differentiation of OSR1(+) FOXD1(+) IPCs, we established OSR1-GFP/FOXD1-tdTomato double-knockin hiPSC lines using our previously reported gene-targeting strategy.[22,23] We constructed the BAC-based vector (Figure 1B), in which a tdTomato reporter gene was knocked in to the FOXD1 locus. The OSR1-GFP knockin hiPSC line, 3D45, which we previously generated,[22] was used as the parental line. One clone, 17K6, was selected as a candidate homologous recombinant with heterozygous tdTomato reporter gene and normal karyotype from 57 drug-resistant clones by a TaqMan quantitative PCR analysis (Item S1, FOXD1_genome; Figure S1G; see method details).

In a previous study using fetal kidneys of P0-Cre mice, kidney fibroblasts in the cortex and outer medulla were mapped with P0-Cre, and most P0-lineage cells were positive for a neural crest marker, p75.[24] However, in another fate-mapping study, Wnt-1 promoter-marked neural crest cells (NCCs) did not enter MM at E11.5.[25] Combining these findings and the reports on Osr1(+) cell-lineage tracing,[6,7] we hypothesized that PPS-derived cells showing Osr1 positivity after E9.5 and a similar identity to NCCs give rise to renal IPCs. Accordingly, we tested several differentiation-inducing conditions on day-6 PPS cells by combining factors that induce NCCs (the ALK inhibitor SB431542 and CHIR99021[26]) or IM and NPCs from PPS (FGF9, NOGGIN, and RA[17]) using 17K6 cells (Figure 1C). Following the original differentiation method for NCCs,[26] we tested 2D culture conditions. Five-day treatment with a combination of CHIR99021 (1 μM), SB431542 (10 μM), and RA

(B) Schematic representation of the targeting strategy to generate FOXD1-tdTomato knockin hiPSC lines. A part of the FOXD1 coding region was replaced with tdTomato and PGK-Neo cassettes. The black boxes represent exon 1 of FOXD1 gene.
(C) Outline of the screening strategy for IPC differentiation from hiPSCs by modifying the last two steps (days 6–8 and 8–11) of our 6-step NPC differentiation protocol.
(D) Flow-cytometry analysis of day-11 cells after treatment with various combinations of NCC- and NPC-induction factors on days 6–11. CHIR99021, 1 μM; SB431542, 10 μM; RA, 0.1 μM; FGF9, 200 ng/mL; Noggin, 25 ng/mL.
(E) Heatmap comparing the expression of reported IPC[27] and PS markers by RNA-seq between hiPSC-derived IPLCs and PPS-like cells, both of which were derived from 17K6. IPLCs were induced in 2D condition using CSR medium and compared with day-6 cells (PPS) in (C).
(F) Flow-cytometry analysis of day-11 cells cultured in 2D or 3D conditions using CSR medium.
(G) Flow-cytometry analysis of day-11 cells treated with or without SAG addition on days 6–8.
Dots and lines in the center of the scatterplots indicate independent experimental data and mean values, respectively, using 17K6 cells (n = 6 in D, n = 10 in F, and n = 10–15 in G). *p < 0.05, **p < 0.01 by Student's t tests in (A), (F), and (G). NS, not significant.

(0.1 μM) together with AK02N minus bFGF medium (CSR medium) induced FOXD1(+) cells at around 40% differentiation efficiency on day 11 (Figure 1D and Item S1 tab 1D). A comparison of induced IPLCs and PPS-like cells by RNA sequencing (RNA-seq) indicated the upregulated expression of several reported IPC marker genes, including *FOXD1*, *TBX18*, and *PBX1*,[27] and the downregulation of PS marker genes, including *TBXT*, *MIXL1*, and *TBX6*, in day-11 IPLCs (Figure 1E and Item S5 tab 1E). However, the cells were not evenly differentiated and formed sparse cell aggregations on the culture plates, suggesting that the differentiation method needed further improvement. Since the NPC induction was improved in 3D floating culture (Figures S1C–S1F), we next tested the same 3D culture condition on days 4–11, finding a higher induction efficiency of FOXD1(+) cells (Figure 1F). Previous reports examining Gli-Luc reporter mice suggested that hedgehog signaling is highly activated in posterior presomitic mesoderm (PSM) between E9.5 and E10.5.[28–30] In addition, an analysis of Gli reporter mice showed that the expression of Gli in Foxd1(+) renal IPCs is high between E11.5 and E14.5.[31] Therefore, we tested the addition of a hedgehog pathway activator, smoothened (SMO) agonist (SAG; 500 nM), to CSR medium on days 6–8, finding it improved the FOXD(+) cell induction efficiency from 58.3% ± 2.8% (n = 10) to 72.6% ± 2.9% (n = 15) (Figure 1G). Taken together, we induced FOXD1(+) IPLCs at around 70% induction efficiency using CSR medium and SAG in 3D floating culture.

Identification of metanephric IPCs in mouse embryos

To investigate the developmental processes of renal IPCs, we performed a single-cell RNA-seq (scRNA-seq) analysis of the caudal trunk parts of E9.5 and E10.5 mouse embryos (Figure S2A). After removing cells of poor quality, 9,357 cells were analyzed. Using a uniform manifold approximation and projection (UMAP),[32] we identified cell clusters corresponding to 18 major cell types (Figure S2B). Although we did not check the biological sex of the embryos, a gene expression analysis of Y chromosomal genes[33,34] and genes related to X chromosome inactivation[33,35] suggested that samples of each embryonic date contain both sexes and that no cell clusters are sex specific (Figure S2C). Genes exhibiting enriched expressions in each cell subset, such as Foxd1 in cluster 2, Tbx6 in cluster 6, and Cited1 in clusters 6 and 7, are shown in Item S2 tab S2B. A gene set enrichment analysis (GSEA) using Metascape for the cluster markers[36] is shown in Table S1. We identified putative PPS and IPC clusters as cluster 6 and clusters 2 and 7, respectively, using these marker genes (Figure S2D, Table S1, and Item S2 tab S2B).

We next performed a reclustering analysis of only PPS and IPCs, which revealed the existence of seven distinct cell clusters (Figures S2E and S2F). Differentially expressed genes (DEGs) in each cell cluster and a GSEA using Metascape for the cluster markers are shown in Item S2 (tab S2G) and Figure S2G, respectively. We confirmed that T(+) PPS clusters (clusters 3 and 4 in Figure S2E) are present only at E9.5 (aqua blue in Figure S2F), while the FOXD1(+) IPC cluster (cluster 0 in Figure S2E) is present only at E10.5 (salmon pink in Figure S2F), suggesting successful identification of the future metanephric IPC cluster.[7] Gene expressions changed from PPS and IM at E9.5 to IPCs at E10.5 through Pax3(+) PSM (Figure S2H), suggesting that PSM plays crucial roles in the PPS-to-IPC transition.[37]

Molecular events during PPS-to-metanephric IPC development

A pseudotime trajectory analysis revealed a linear trajectory of PPS to IPCs through PSM from E9.5 to E10.5 (Figures 2A and 2B). Five patterns of gene expression dynamics were identified and clustered along the pseudotime trajectory (Figure 2C and Item S2 tab 2C). To define signaling pathways temporally regulated during the IPC transition, we used Ingenuity Pathway Analysis (IPA) to predict which signaling pathways are activated in cells transitioning to IPCs (Figure 2C). We confirmed activation of the SHH pathway during the IPC transition (Item S3), which is consistent with the results of our IPLC induction (Figure 1G) and previous reports.[28,31] Taken together, our analysis captured the molecular signatures of differentiation from PPS to IPC in mice.

Improvement of IPLC-induction efficiency by interleukin-1β

To improve our IPLC induction, we targeted the signaling pathways through PPS to IPCs, especially upregulated pathways near the IPC state transition (clusters 2, 3, and 5 in Figure 2C). The IPA results from IPC-transitioning cells suggested an upregulation of the WNT/Ca^{2+} pathway, estrogen receptor signaling, hepatic fibrosis, and interleukin-1 (IL-1) signaling (Figure 2C and Item S3). We thus tested the addition of WNT3a and RSPO1, β-estradiol, transforming growth factor β1 (TGF-β1), or IL-1β to CSR medium with SAG on days 6–8 and to CSR medium with or without SAG on days 8–11, confirming that the addition of IL-1β (10 ng/mL) on days 6–8 (Figure 3A, yellow; Figure S3A; Item S1 tab 3A) and SAG (500 nM) on days 6–11 (CSR+SI+S) produced the highest induction efficiency of OSR1(+)FOXD1(+) cells (Figure S3B, light blue; Item S1 tab S3B). We further confirmed that several ALK inhibitors instead of SB431542 on days 6–11 induce IPC markers as well and that the *MEIS1* expression is significantly downregulated without RA on days 6–11 (Figure S3C and Item S1 tab S3C). We also confirmed that AK02N minus bFGF medium in the CSR medium can be replaced with NPC basal medium (see method details). A GSEA of DEGs from the RNA-seq analysis in the absence or presence of RA showed an upregulation of the cell-type signature gene set of kidney stromal cells[36,38,39] when RA is present (Figure S3D and Item S5 tab S3D).

We also confirmed that our IPLC-induction method is applicable to another hiPSC line, Ff-I 14s04[40] (Figures S3E and S3F; Item S1 tab S3E). As mentioned above, protocols vary in their use of BMP inhibitors[19] and duration of CHIR99021 treatment[18] for the induction of late PS, which contributes to MM lineages. Accordingly, we found that 1383D2, 1383D6, and 201B7 cells require LDN-193189 (100 nM) on day 3 and that 1231A3 cells require an optimized CHIR99021 treatment that omits stage 2 to induce FOXD1(+) cells (Figures 3B, 3C, and S3G). In addition, we found that day-4 cells (upon reseeding) can be frozen and rethawed to induce either IPLCs or NPCs (Figures 3D, S3H, and S3I). Accordingly, we showed the importance of SHH

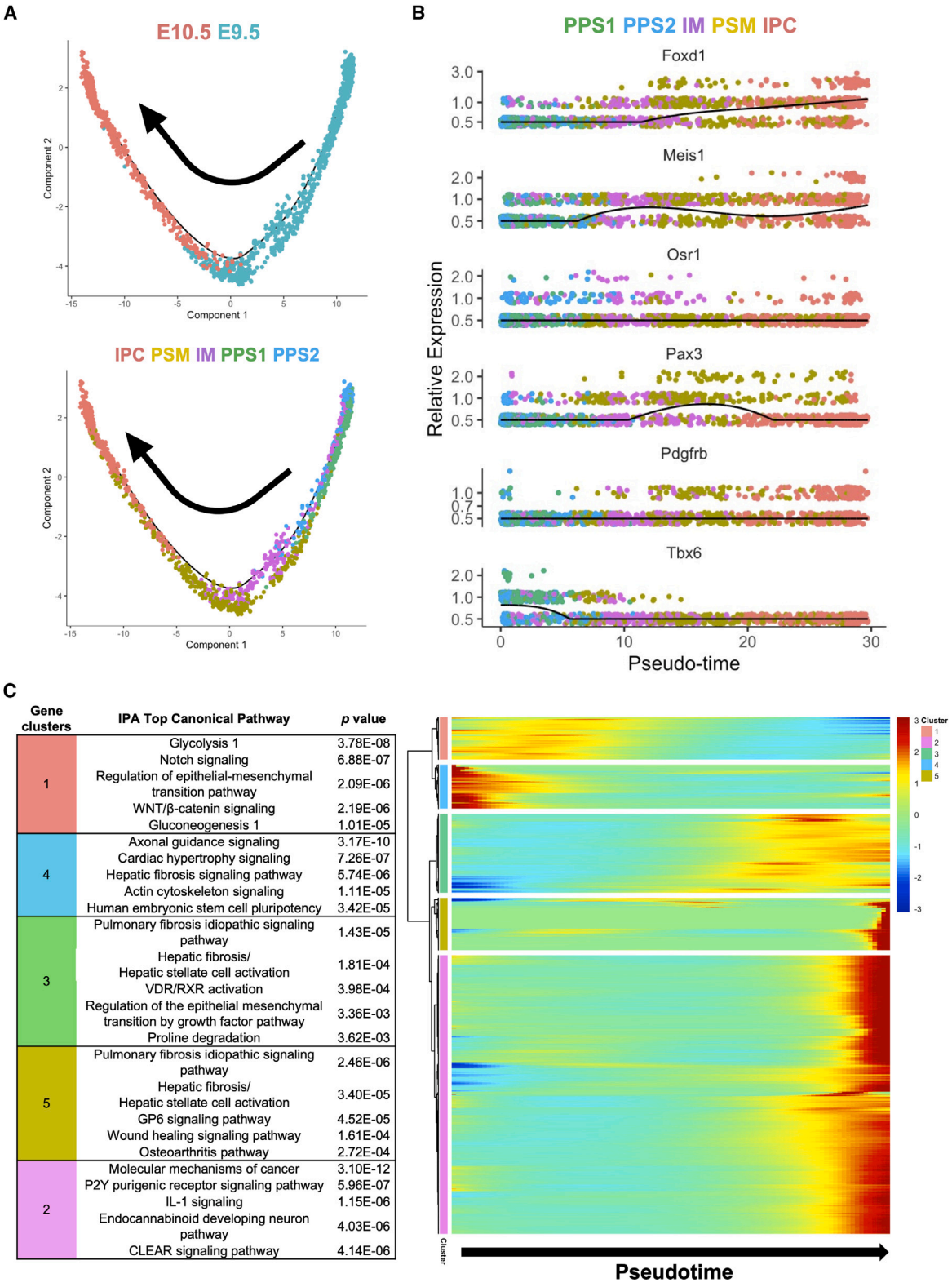

Gene clusters	IPA Top Canonical Pathway	*p* value
1	Glycolysis 1	3.78E-08
	Notch signaling	6.88E-07
	Regulation of epithelial-mesenchymal transition pathway	2.09E-06
	WNT/β-catenin signaling	2.19E-06
	Gluconeogenesis 1	1.01E-05
4	Axonal guidance signaling	3.17E-10
	Cardiac hypertrophy signaling	7.26E-07
	Hepatic fibrosis signaling pathway	5.74E-06
	Actin cytoskeleton signaling	1.11E-05
	Human embryonic stem cell pluripotency	3.42E-05
3	Pulmonary fibrosis idiopathic signaling pathway	1.43E-05
	Hepatic fibrosis/ Hepatic stellate cell activation	1.81E-04
	VDR/RXR activation	3.98E-04
	Regulation of the epithelial mesenchymal transition by growth factor pathway	3.36E-03
	Proline degradation	3.62E-03
5	Pulmonary fibrosis idiopathic signaling pathway	2.46E-06
	Hepatic fibrosis/ Hepatic stellate cell activation	3.40E-05
	GP6 signaling pathway	4.52E-05
	Wound healing signaling pathway	1.61E-04
	Osteoarthritis pathway	2.72E-04
2	Molecular mechanisms of cancer	3.10E-12
	P2Y purigenic receptor signaling pathway	5.96E-07
	IL-1 signaling	1.15E-06
	Endocannabinoid developing neuron pathway	4.03E-06
	CLEAR signaling pathway	4.14E-06

Figure 2. Molecular events during transition from PPS to metanephric IPCs

(A) Pseudotime trajectory analysis of PPS, IM, PSM, and IPC clusters. Upper: clusters segregated by gestational age. Lower: PPS, IM, PSM, and IPC clusters.

(B) Expression pattern of marker genes for IPCs (Foxd1, Meis1, and Pdgfrb), IM (Osr1), PSM (Pax3), and PPS (Tbx6) along the pseudotime axis.

(C) Heatmap of DEGs during the transition from PPS to IPCs following the trajectory timeline shown in (A). Left: activated canonical pathways predicted by IPA based on each clustered DEG. Right: DEGs clustered by their expression patterns.

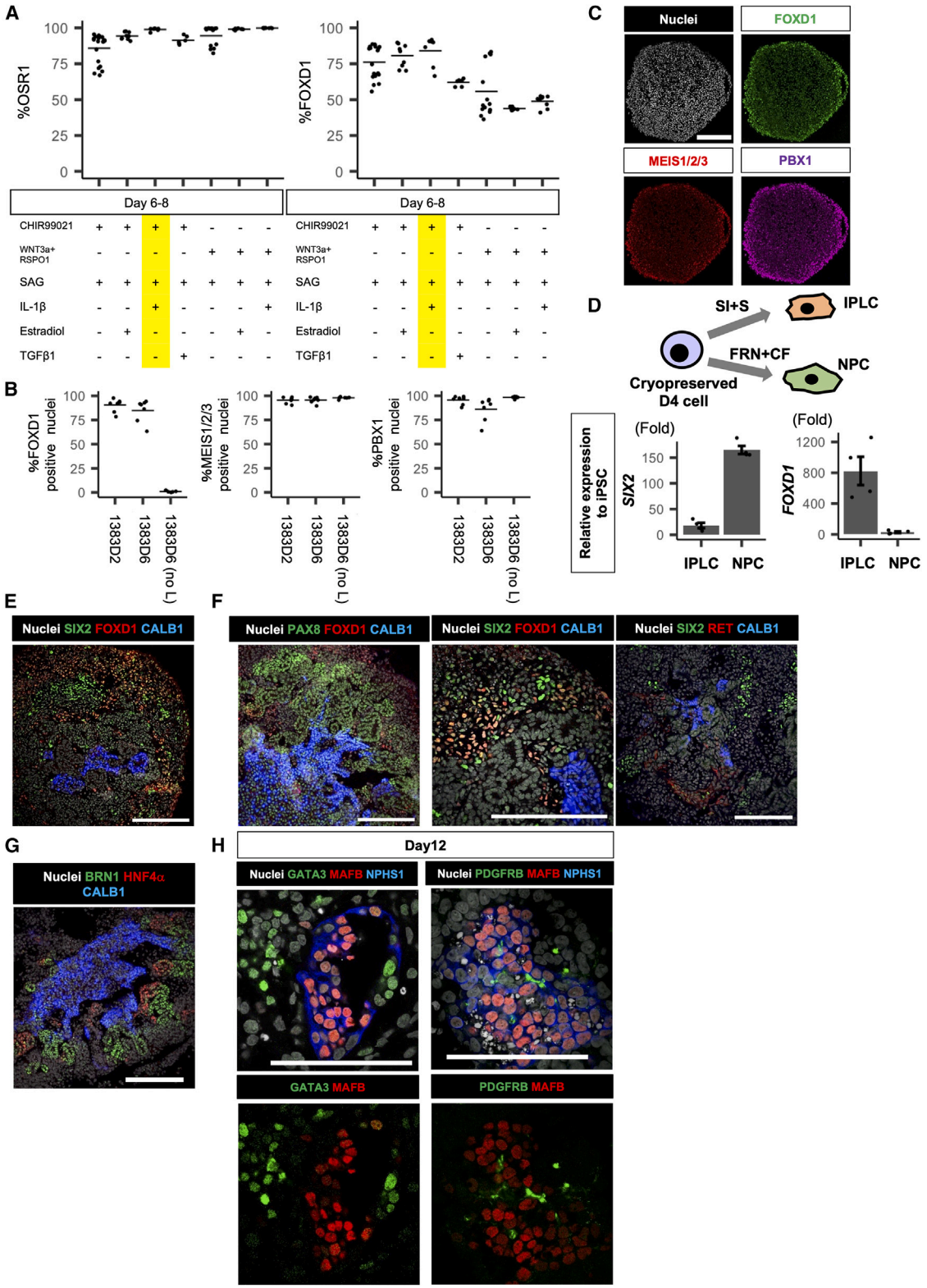

Figure 3. Efficient induction of IPLCs from hiPSCs

(A) Screening for combinations of inducing factors identified by analyzing mouse embryos on days 6–8. CHIR99021, 1 μM; WNT3a and RSPO1, 10% WNT3a and afamin conditioned medium and 200 ng/mL RSPO1; SAG, 500 ng/mL; IL-1β, 10 ng/mL; estradiol, 50 ng/mL; TGF-β1, 10 ng/mL.

(legend continued on next page)

signaling, IL-1β, and RA in the induction of IPLC from hiPSCs (Figure 7I).

IPLCs form nephrogenic niche- and mesangium-like structures

In kidney development, NPCs promote ND budding and induce UB, while NPCs and IPCs create cap mesenchyme that surrounds UB.[41] To test the function of our induced IPLCs, we co-cultured hiPSC-derived NPCs, IPLCs, and ND cells (NDCs). We previously reported that the co-culture of hiPSC-derived single NPCs and NDCs on day 9 of the UB induction protocol[42] recapitulates nephrogenesis *in vitro*.[17] Another study using Matrigel embedding achieved complex tree-like kidney structures from mouse ESC-derived NPCs, IPCs, and UB cells.[8] Similarly, we mixed and co-cultured hiPSC-derived NPCs, IPLCs, and NDCs in Matrigel-embedded conditions supplemented with CHIR99021 (1 μM), RA (0.1 μM), FGF9 (200 ng/mL), and Y-27632 (10 μM; CRFY), which are used in our NPC- and IPLC-induction protocols. Consequently, CALB1(+) epithelial structures were reconstructed, and SIX2(+) NPCs and FOXD1(+) IPLCs surrounded UB-like epithelial structures in the aggregates (Figure 3E). However, RET expression was not detected in UB tip-like structures. Therefore, we tested inducing factors used in our previously reported UB tip cell-expansion culture.[42] Under conditions with a higher concentration (3 μM) of CHIR99021 (C3RFY), the expression of *WNT11* increased but the expression of *SIX2* decreased. When GDNF (200 ng/mL) was added (CRFY+G), *RET* expression was elevated without affecting other progenitor markers, such as *SIX2* and *FOXD1* (Figure S4A and Item S1 tab S4A). In addition, we previously reported that when CHIR99021 is replaced with Wnt3a conditioned medium and R-spondin1 protein (RSPO1), UB tip and trunk formation improves.[42] Accordingly, we added Wnt3a conditioned medium (10%) and RSPO1 (200 ng/mL; RFY+G+WR), which further increased *RET* expression (Figure S4B and Item S1 tab S4B). Immunostaining showed that budding UB tips were positive for RET (Figure 3F) and that nephrogenic niche-like structures, such as SIX2(+) or PAX8(+) cap mesenchyme-like structures (Figures 3F and S4C) and S-shaped body-like structures consisting of HNF4α(+) proximal and BRN1(+) distal and medial segments, were formed (Figure 3G).

Mesangial cells derived from Foxd1(+) IPCs migrate into developing glomerular tufts. In glomeruli at the capillary loop stage, podocytes surround Pdgfrb(+) mesangial cells and then form mesangium structures.[43] Consistently, we found glomerulus-like structures with PDGFRB(+) or GATA3(+) mesangium-like cells at the capillary loop stage on days 6 and 12 and at the maturation stage on day 12 in organoids (Figures 3H and S4D). To distinguish the origin of mesangium-like structures, we co-cultured IPLCs induced from a 201B7-derived hiPSC line constitutively expressing EGFP (317-12 cells)[44] and non-fluorescent NPCs under RFY+G+WR medium condition. Consequently, we confirmed glomerulus-like structures with EGFP(+) PDGFRB(+) mesangium-like structures on day 6 (Figure S4E). The expression pattern of mesangial markers is different between humans and mice.[45] Therefore, we examined the mesangial marker expression of E57 cynomolgus monkey kidneys as a primate alternative to developing human kidneys (Figure S4F). The PDGFRB and GATA3 expression was positive in mesangial structures, although the strength of the PDGFRB expression varied among glomerular developmental stages. DESMIN expression was weak or absent, which is consistent with human mesangium.[45]

These results suggest that our IPLCs can form nephrogenic niche- and mesangium-like structures when combined with hiPSC-derived NPCs and NDCs, although, unlike mice, they require exogenous factors in the culture for unknown reasons. A longer incubation did not yield extensive tree-like structures, indicating that improvements in the culture conditions are needed.

IPLCs can differentiate into various embryonic kidney stromal lineages

To further define the identity of our hiPSC-derived IPLCs, we performed scRNA-seq analysis to compare IPLCs, stromal subsets of human embryonic kidney tissue[46] (HEK; Figure 4A), and stromal subsets of day-12 kidney organoids generated from hiPSC-derived IPLCs, NPCs, and NDCs (Figure 4B). Although there were differences in the single-cell gene expression library preparation and the number of genes detected between our datasets (10× Genomics v3.1 reagent) and a publicly available HEK dataset (10× Genomics v3 reagent; Figure S4G), IPLCs showed a similar expression pattern of FOXD1 but additionally expressed the early multipotent stromal marker TBX18[8,47] (Figure 4C), suggesting that IPLCs represent early IPCs equivalent to those in E11.5 mouse metanephros[8,47] and have a different expression pattern of reported stromal marker genes[11] from stromal (or interstitial) progenitor cells (SPCs) in HEK (gestational days 96 and 108) (Figure 4D and Item S2 tab 4D). On the other hand, the stromal subsets (SPC, cortical stroma, medullary stroma, and mesangial cells) of day-12 kidney organoids generated

(B and C) Percentage (%) of FOXD1(+), MEIS1/2/3(+), or PBX1(+) cells (B) and representative images of section immunostaining of an hiPSC (1383D6)-derived IPLC aggregate for FOXD1, MEIS1/2/3, and PBX1 (C).

(D) RT-qPCR analysis of 1231A3-derived day-11 cells differentiated from cryopreserved day-4 cells induced with PPS and then CSR+SI+S condition (for IPLCs) or FRN+CF condition (for NPCs) for *FOXD1* (IPCs) and *SIX2* (NPCs).

(E–H) Immunostaining of kidney organoids from hiPSC-derived NPCs, IPLCs, and NDCs on day 6 after treatment with CRFY (E) and RFY+G+WR medium (F and G) and on day 12 after treatment with RFY+G+WR medium (H). CALB1 and RET (UB), PAX8 (renal vesicle or S-shaped bodies), BRN1 and HNF4α (S-shaped bodies), NPHS1 and MAFB (podocytes), and PDGFRB and GATA3 (mesangial cells). Scale bars, 200 μm (C and E–G) and 100 μm (H).

Dots and lines in the center of the scatterplots indicate independent experimental data and mean values, respectively, using 17K6 cells (n = 6–20) in (A) and 1383D2 or 1383D6 cells (n = 3–8) in (B). Data are presented as the mean ± SEM, and dots indicate independent experimental data using 1231A3 cells (n = 4) in (D). Representative data from independent experiments using a combination of 201B7-derived NPCs and IPLCs and 1231A3-derived NDCs (n = 3 in E and H, n = 4 in F and G). FRN+CF, basal medium supplemented with 200 ng/mL FGF9, 100 nM RA, and 25 ng/mL Noggin followed by basal medium supplemented with 1 μM CHIR99021 and 200 ng/mL FGF9.

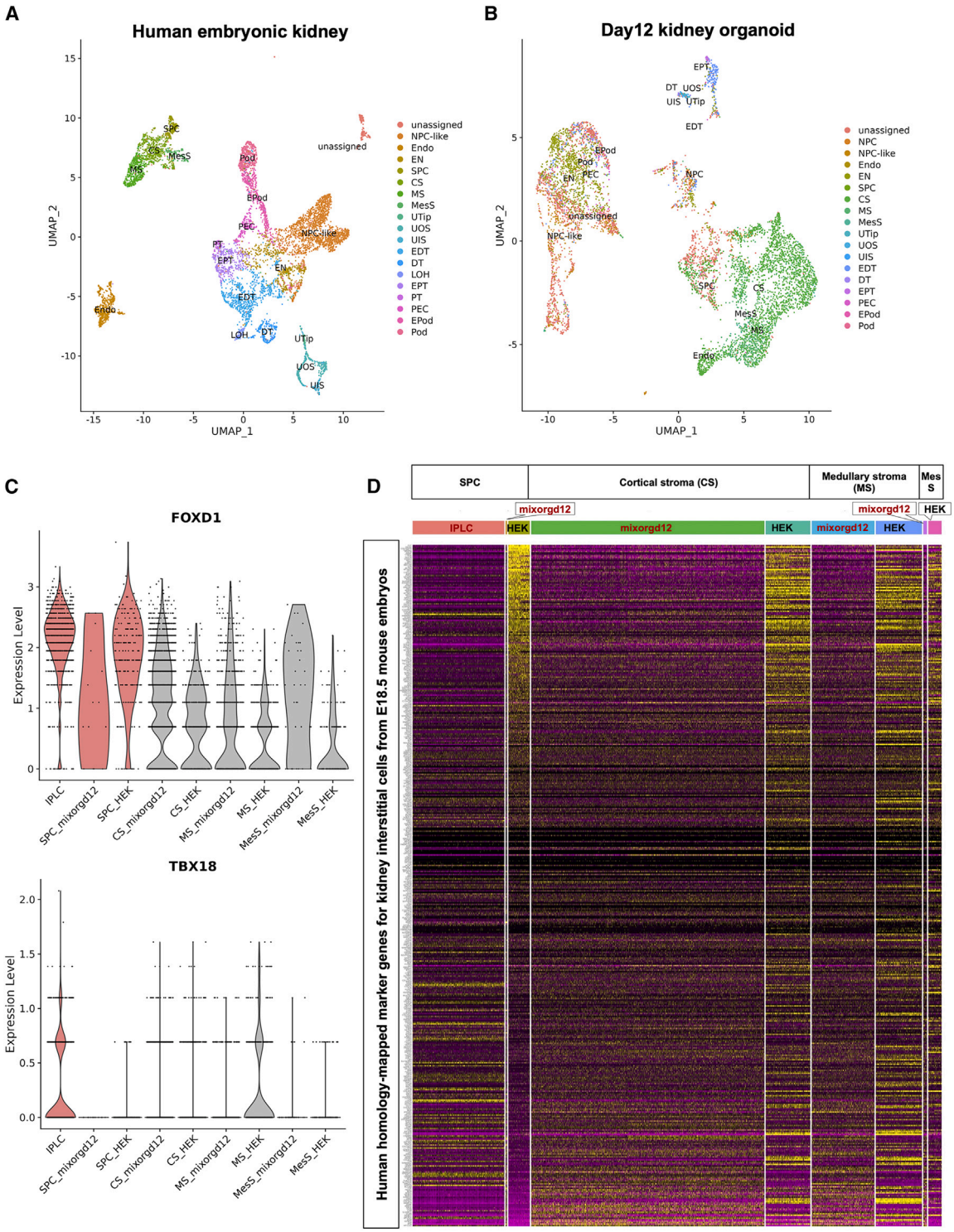

Figure 4. scRNA-seq analysis of day-12 kidney organoids generated from hiPSC-derived IPLCs, NPCs, and NDCs

(A and B) UMAP representation of DevKidCC classification of HEK (gestational days 96 and 108, E-MTAB-9083; A) and day-12 kidney organoids generated from hiPSC-derived IPLCs, NPCs, and NDCs (B).

(C) Violin plots showing expression of FOXD1 and TBX18 by hiPSC-derived IPLCs (IPLC); by stromal subsets of day-12 kidney organoids from hiPSC-derived IPLCs, NPCs, and NDCs (mixorgd12); and by stromal subsets of HEK (gestational days 96 and 108, E-MTAB-9083; HEK) annotated by DevKidCC.

(legend continued on next page)

from IPLCs, NPCs, and NDCs exhibited a gene expression pattern closer to that of stromal subsets of the reported HEK (Figure 4D). We annotated these cell types using DevKidCC.[48] These data suggest that when co-cultured with NPCs and NDCs *in vitro*, IPLCs demonstrated the ability to differentiate into various embryonic kidney stromal lineages, again supporting their status as IPCs.

ALK5 inhibition is crucial for differentiation of IPLCs to mesangial and EPO-producing cell lineages

We examined whether IPLCs can differentiate into mesangial and EPO-producing cell lineages *in vitro*. A previous report suggested a prolyl hydroxylase domain inhibitor, FG-4592, and RA increase EPO production in adult kidney.[49] Under 5% O_2 hypoxic conditions with FG-4592 (10 μM) and RA (100 nM), we screened IPLC-induction factors by measuring *EPO* and *RENIN* expression. Consequently, with a low concentration (1 μM) of CHIR99021, SB431542 (10 μM) increased the expression of *RENIN* in the absence of SAG, and a combination of SB431542 and SAG (500 nM) upregulated *EPO* expression (Figure S5A and Item S1 tab S5A). To further investigate the effects of ALK inhibition, we screened TGF-β family proteins and ALK inhibitors and found that TGF-β1 downregulated both *EPO* and *RENIN* expression, BMP7 (10 ng/mL) had positive effects on *RENIN* expression in the absence of SAG, and a combination of A83-01 (1 μM) and SAG produced higher *EPO* expression than the combination of SB431542 and SAG (Figure S5B and Item S1 tab S5B). These data indicate that IPLCs can differentiate into mesangial and EPO-producing cell lineages *in vitro*.

BMP and ALK5 inhibitor upregulate p38 MAPK signaling upon mesangial-lineage differentiation

BMP4, BMP5, and BMP7 are required for kidney development.[50–54] We thus tested the effects of these BMPs with or without SB431542 in CHIR99021, FG-4592, and RA (CFR) media and found that any of the three BMPs (100 ng/mL) had positive effects on *RENIN* expression with SB431542 (Figures 5A and 5B; Item S1 tabs 5A and 5B). Because a previous report showed the importance of Notch signaling for the differentiation of mesangial cells from IPCs,[55] we also tested two Notch signaling agonists, JAG and DLL4, and the inhibitor DAPT but found no significant effects on *RENIN* expression (Figures 5B and S5C; Item S1 tabs 5B and 5C).

GATA3 plays crucial roles in mesangial and juxtaglomerular (JG) cell development, and GJA5 is a mesangial cell marker.[45,56,57] We confirmed the upregulated expression of *GATA3*, *RENIN*, and *GJA5* and downregulation of *FOXD1* after a 96-h treatment with CFR medium containing BMP7 and SB431542 (CFR+B7+SB medium) (Figure 5C). Consistently, immunostaining revealed two cell types in the aggregates: GATA3(+) and RENIN(+/high) cells (Figures 5D and 5E).

To examine whether CFR+B7+SB medium also induce *Renin* expression in mice, we performed organ cultures of E13.5 mouse metanephroi. Although there was no apparent difference in the size of metanephroi after a 48-h culture (Figure 5F), *Renin* expression was upregulated similarly with CFR+B7+SB medium and the expression of feedback factors in the SMAD pathway (*Smad6* and *Smad7*), which is the canonical pathway of BMPs,[58–60] did not change (Figure 5G). Therefore, we analyzed p38 MAPK, a crucial molecule of the non-Smad pathway and reported as essential for nephrogenesis and kidney growth,[61] finding its phosphorylation was upregulated in our human mesangial-lineage induction system (Figure 5H). Furthermore, using a p38 MAPK inhibitor, SB203580, the expression of *RENIN*, but not *GJA5*, *GATA3*, or *FOXD1* was downregulated (Figure 5I and Item S1 tab 5I). We also found that an RAR agonist, TTNPB, upregulates *RENIN* expression, similar to RA, while the addition of two antagonists, BMS493 and AGN 193109, reverses this effect (Figure S5D and Item S1 tab S5D). *RENIN* expression changed over time, and a high expression level was maintained after 72 h (Figure S5E).

These results indicate that the upregulation of p38 MAPK signaling induces *RENIN* expression and the involvement of RA signaling in mesangial-lineage cell development *in vitro*.

p38 MAPK is activated in mesangial lineages of GW14 HEK

To elucidate the roles of p38 MAPK signaling in *in vivo* mesangial-lineage development, we examined molecular signals for the differentiation of renin-producing cells from IPCs using openly available single-cell transcriptome data of GW14 HEK cortex.[62] Cluster classification using DevKidCC[48] identified stromal clusters including RENIN(+) cells as mesangial-lineage cells (Figures S6A–S6D). Immunostaining E57 cynomolgus monkey kidneys also confirmed the existence of GATA3(+)RENIN(−) and GATA3(+)RENIN(+) mesangial cells in developing glomeruli (Figure S6E). To understand the transcriptomic dynamics upon the transition from IPCs to mesangial cells, we examined IPCs (cluster 0 in Figure S6B) transitioning to the mesangial-lineage cluster (cluster 5 in Figure S6B) by a pseudotime analysis (Figure 6A). A DEG analysis along the branch of the trajectory showed *GATA3* upregulation in cluster 5 followed by *RENIN* upregulation (Figures 6B and S6F; Item S2 tab 6B). A pathway analysis confirmed Notch signaling activation upon the mesangial cell transition[55] and revealed transcriptional changes related to p38 MAPK signal activation in the transition to cluster 5 (Figure 6B and Item S4).

Renin-producing cell precursors originate from Foxd1(+) cells and commit to both mesangial and JG cells in murine kidney development.[63] Gata3(+)Foxd1(+) cells commit to renin-producing and mesangial cells.[56] Therefore, we examined mesangial- and JG-lineage cells in detail by dividing cluster 5 into

(D) Heatmap comparing expressions of human homology-mapped marker genes for kidney interstitial cells from E18.5 mouse embryos[11] with IPLC, stromal subsets of mixorgd12, and stromal subsets of HEK. The gene order was arranged based on the high average expression values of the HEK SPC subset. Note that the SPC and MesS subsets of mixorgd12 contain 15 and 40 cells, respectively.

NPC, nephron progenitor cell; Endo, endothelium; EN, early nephron; SPC, stromal (or interstitial) progenitor cell; CS, cortical stroma; MS, medullary stroma; MesS, mesangial cells; UTip, ureteric tip; UOS, ureteric outer stalk; UIS, ureteric inner stalk; EDT, early distal tubule; DT, distal tubule; LOH, loop of Henle; EPT, early proximal tubule; PT, proximal tubule; PEC, parietal epithelial cell; EPod, early podocyte; Pod, podocyte.

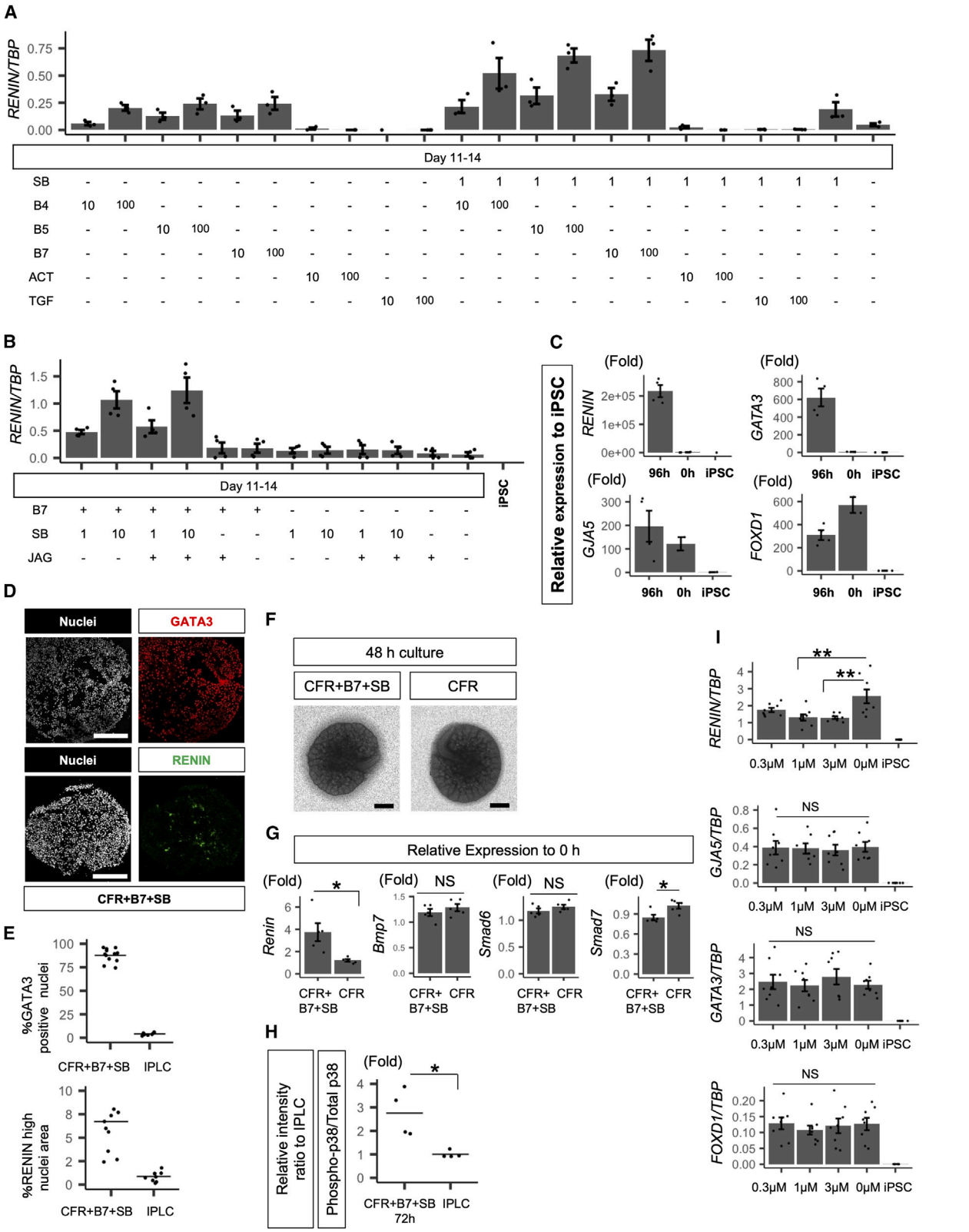

(legend on next page)

subclusters (c5-0, c5-1, c5-2, and c5-3) (Figures S6G, S7A, and S7B). The analysis of DEGs and reported adult JG and mesangial marker genes[64] suggested that cluster 5 contains both mesangial (c5-1) and JG/SMC cells (c5-2) (Figures S7B and S7C; Item S2 tab S7C1) and a similar developmental origin of both cells in human kidney development.

These data from *in vitro* experiments using IPLCs and the analysis of *in vivo* GW14 HEK suggest that in mesangial and JG cell development, FOXD1(+) IPCs differentiate to RENIN(+) mesangial-lineage cells with p38 MAPK signal activation.

Hypoxia-related signals are activated in JG cell lineages of GW14 HEK

To further investigate developmental mechanisms of mesangial and JG cells, in addition to comparing DEGs for each cluster we examined signaling pathways related to DEGs between c5-1 and c5-2, finding hypoxic signal activation in the JG cell cluster (Figure S7C and Item S2 tab S7C2). Since mesangial and JG cell development are associated with endothelial cells and hypoxic signaling is related to vascular endothelial growth factor (VEGF),[65] we tested VEGF (100 ng/mL) and its receptor inhibitor axitinib (3 μM). The addition of VEGF to CFR+B7+SB medium enhanced both JG and mesangial marker expression, but the effect was reversed by axitinib (Figure 6C and Item S1 tab 6C). Compared to VEGF, the effects of oxygenic condition (CFR+B7+SB medium under 5% O_2 vs. CFR+B7+SB medium minus FG-4592 under 20% O_2) were minimal. We also confirmed that the amount of RENIN protein in culture supernatants and the rate of RENIN(+) cells in the aggregates were increased with treatment of CFR+B7+SB medium plus VEGF (CFR+B7+SB+V) compared to CFR+B7+SB medium plus axitinib (Figures S7D and S7E). When culture supernatants of the cell aggregates were reacted with renin substrate, angiotensin I production was detected, confirming renin activity. An RNA-seq analysis also suggested the upregulation of JG/SMC and mesangial markers compared to IPLCs when IPLCs were treated with CFR+B7+SB+V medium under hypoxic conditions (5% O_2; hypoxia) or with CFR+B7+SB+V medium minus FG-4592 under normoxic condition (minus FG-4592 and under 20% O_2; normoxia) (Figure S7F and Item S5 tab S7F). These findings suggest that VEGF signals are involved in mesangial-lineage development.

SHH signal agonists induce EPO expression

Since SAG and A83-01 induced *EPO* expression (Figure S5B and Item S1 tab S5B), we examined the effects of SHH modulators in combination with CFR medium supplemented with A83-01 (CFR+A83 medium) under hypoxic conditions (5% O_2) to differentiate IPLCs into EPO-producing cells. Under inactive states of SHH signaling, SMO is repressed by hedgehog receptor patched (PTC), while upon SHH binding to PTC the repression is inhibited to activate SHH signaling.[66] The processing and nuclear translocation of the zinc finger protein GLI also plays key roles in the SHH signaling cascade. We therefore tested several SMO antagonists (sonidegib, vismodegib, and SANT-1) and agonists (SAG and purmophamine), a GLI1 inhibitor (GANT61),[67] and human SHH protein (Figure 7A). We found that both SMO agonists and human SHH protein upregulated *EPO*. Human SHH protein (100 ng/mL) alone produced the highest expression, whereas all SMO antagonists but not the GLI1 inhibitor reversed the effects of SAG (Figure 7A and Item S1 tab 7A). An RT-qPCR analysis showed that *EPO* expression reached its peak after about 96 h of treatment with CFR+A83 medium supplemented with SHH protein (CFR+A83+SHH) (Figure 7B). These findings suggest that IPLCs can differentiate into EPO-producing cells through SHH activation.

We next examined whether EPO is secreted in response to physiological stimuli such as hypoxia. Immunoassays showed that significantly more EPO protein was secreted into culture medium after 4-day hypoxic incubation with CFR+A83+SHH treatment compared to normoxic conditions (Figure 7C). An RT-qPCR analysis showed *EPO* upregulation in IPLCs treated with CFR+A83+SHH medium compared to hiPSC-derived NPC kidney organoids after 4-day hypoxic incubation (Figure 7D). In addition, we successfully concentrated EPO protein secreted into the culture medium using ultrafiltration membranes with pore sizes that select for substances above 30 kDa (Figure 7E) and performed clonogenic hematopoietic progenitor assays using methylcellulose-based semisolid media. We measured the number of clonal colonies on semisolid medium containing stem cell factor (SCF), granulocyte macrophage colony-stimulating factor (GM-CSF), IL-3, IL-6, and granulocyte colony-stimulating factor (G-CSF) supplemented with induced cell-derived EPO protein (iEPO protein, 0.2 and 2.0 IU/mL), finding that iEPO protein induces erythroblast cells (Figure 7F) but is neutralized by anti-human EPO antibodies (Figure 7G).

Figure 5. Induction of IPLCs toward RENIN(+) mesangial-lineage cells

(A and B) RT-qPCR analysis of *RENIN* expression. CFR medium with higher concentrations of BMPs (100 ng/mL) and SB431542 (1 μM) (A) or higher concentrations of SB431542 (10 μM) and BMP7 (100 ng/mL) (B) on days 11–14 significantly upregulated the *TBP*-normalized gene expression of *RENIN*.

(C) RT-qPCR analysis of *RENIN*, *GJA5*, and *GATA3* (mesangial lineages) and *FOXD1* at 0 h and 96 h after CFR+B7+SB treatment.

(D and E) Section immunostaining images of an IPLC aggregate treated with CFR+B7+SB for 72 h for GATA3 and RENIN (D) and quantification of the percentage (%) of GATA3(+) or REN (+/high) cells (E). Note that RENIN signals were observed in both the cytoplasm and nucleus.

(F and G) Bright-field images of E13.5 mouse metanephros treated with CFR+B7+SB or CFR alone in organ cultures for 48 h (F), and RT-qPCR analysis of *Renin* and negative feedback molecules downstream of the canonical BMP pathway (*Bmp7*, *Smad6*, and *Smad7*) (G). The values were normalized to that of E13.5 mouse metanephros.

(H) The ratio of p38 MAPK (p38) and phosphorylated p38 MAPK (phospho-p38) expression levels. The values in the scatterplot indicate the area under the curve of the phospho-p38 signals normalized to that of the corresponding total p38 proteins. The values were then normalized to that of IPLCs.

(I) RT-qPCR analysis of expressions for *RENIN*, *GJA5*, *GATA3*, and *FOXD1*.

Data are presented as the mean ± SEM, and dots indicate independent experimental data using 17K6 cells (n = 3 in A, n = 4 in B and C, n = 5 in G, and n = 8 in I). Dots and lines in the center of the scatterplots indicate experimental data and mean values, respectively, using 17K6 cells (n = 9 in E and n = 4 in H). The units of activin, TGF-β1, and JAG1 are ng/mL in (A) and (B). Scale bars: 200 μm (D) and 500 μm (F).

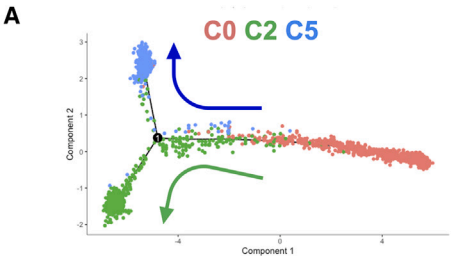

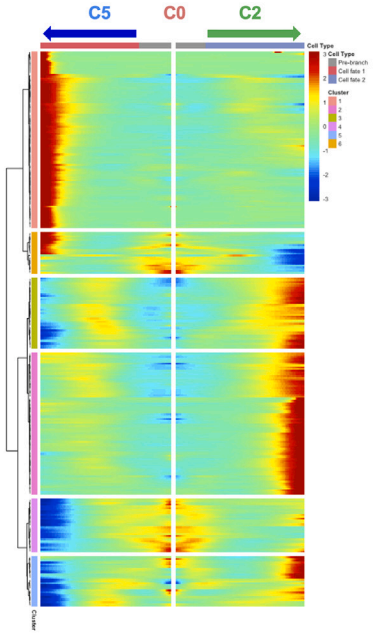

Gene clusters	IPA Top Canonical Pathway	*p* value
1	Notch Signaling	2.05E-05
	Cardiomyocyte Differentiation via BMP Receptors	4.29E-03
	LPS/IL-1 Mediated Inhibition of RXR Function	4.66E-03
	Clathrin-mediated Endocytosis Signaling	9.40E-03
	p38 MAPK Signaling	1.41E-02
6	Dilated Cardiomyopathy Signaling Pathway	4.38E-04
	Calcium Signaling	1.31E-03
	Role of NFAT in Cardiac Hypertrophy	1.42E-03
	SPINK1 General Cancer Pathway	2.21E-03
	α-Adrenergic Signaling	5.31E-03
3	Human Embryonic Stem Cell Pluripotency	2.56E-03
	CREB Signaling in Neurons	2.97E-03
	Pulmonary Healing Signaling Pathway	4.26E-03
	RHOGDI Signaling	5.28E-03
	G-Protein Coupled Receptor Signaling	5.58E-03
2	Hepatic Fibrosis / Hepatic Stellate Cell Activation	3.88E-06
	GP6 Signaling Pathway	8.64E-04
	Cardiac β-adrenergic Signaling	2.98E-03
	Wound Healing Signaling Pathway	1.00E-02
	Apelin Endothelial Signaling Pathway	1.17E-02
4	Pulmonary Fibrosis Idiopathic Signaling Pathway	5.12E-05
	Tumor Microenvironment Pathway	7.38E-05
	Hepatic Fibrosis / Hepatic Stellate Cell Activation	1.01E-04
	Wound Healing Signaling Pathway	2.75E-04
	Axonal Guidance Signaling	4.05E-04
5	Role of Tissue Factor in Cancer	8.83E-03
	Adipogenesis pathway	1.18E-02
	Prostanoid Biosynthesis	1.22E-02
	Regulation Of The Epithelial Mesenchymal Transition By Growth Factors Pathway	2.29E-02
	Hepatic Fibrosis / Hepatic Stellate Cell Activation	2.34E-02

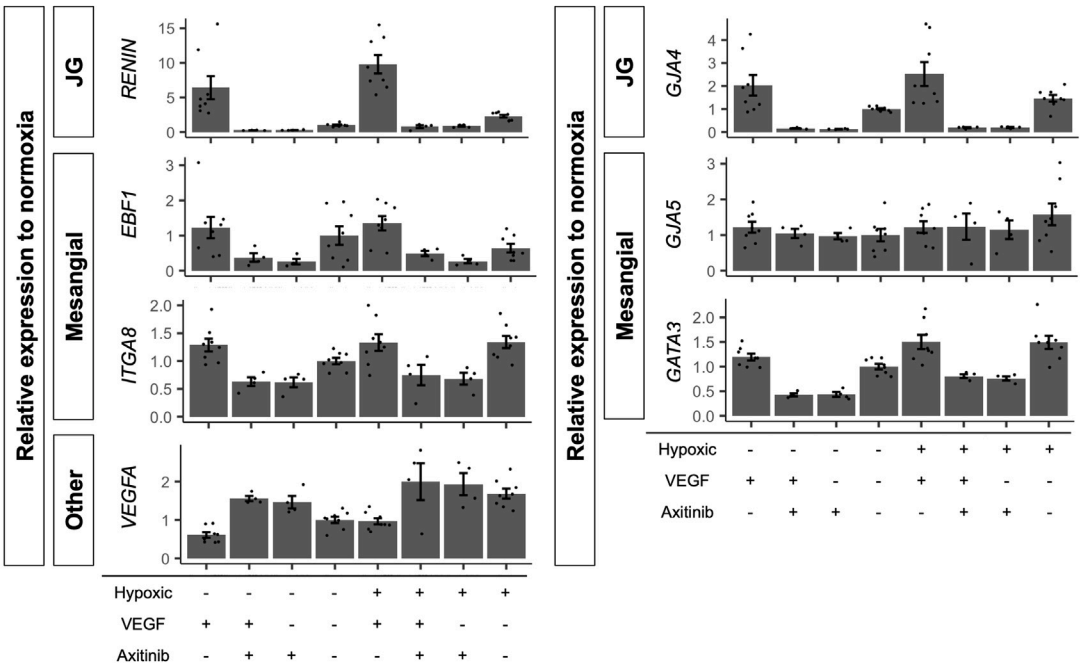

(legend on next page)

Accordingly, we developed a system that separately induces hiPSC-derived IPLCs into mesangial and EPO-producing cell lineages (Figures 7H and 7I).

DISCUSSION

By selectively generating a single lineage, it becomes possible to elucidate developmental signals in detail with regard to complex organ development. We here revealed developmental signals of mesangial lineages, such as p38 MAPK. This finding is significant, as it offers insights that cannot be obtained through simultaneous induction approaches. Moreover, we induced mesangial structures in the glomeruli of organoids *in vitro*. In previously reported kidney organoids generated by simultaneous induction approaches, the majority of PDGFRB(+) stromal cells were present in the periphery of organoids,[68] and PDGFRB(+) mesangial structures were not observed.[15,69–72]

While a recent report induced renal IPCs from mouse ESC-derived ROBO2(+)PDGFRA(+)-sorted mesodermal cells by treatment with FGF9, RA, LDN-193189, SHH, and Y-27632,[8] we selectively induced renal IPLCs from hiPSC-derived PPS cells, which were generated using our previously reported NPC differentiation method, by treatment with CHIR99021, SAG, SB431542, IL-1β, and RA. Our method requires no purification by flow cytometry to generate IPLCs. However, the importance of SHH signaling, RA, and ALK inhibitors for stromal induction is consistent between the two methods. Additionally, our data fit well with previous studies reporting that the addition of IL-1β in the culture media promotes stromal cell proliferation in kidney organoids[73] and that Wnt signaling is involved in embryonic stroma development.[74,75]

While the cell fate of PS depends on the spatial location and developmental stage,[76,77] PPS reported in Takasato et al.[78] and in our current and previous studies[17] represent cells closer to T(+) posterior nascent mesoderm reported in Taguchi et al.[9] and T(+)Tbx6(+) mesodermal precursors in Hayashi et al.,[79] because the cells all express PS markers and give rise to posterior IM and subsequent MM lineages. We induced cells positive for the posterior markers HOXC10[80] and HOXA11[81] and the PPS markers T, TBX6, and CITED1 (MSG1)[82] and showed that such cells exist in E9.5 mouse embryos by scRNA-seq analysis. Therefore, these data suggest our method induces MM-committed PPS from hiPSCs.

Tanigawa et al. showed that IPCs are crucial for the formation of higher-order structures in mouse kidneys and successfully induced mesangial cells by transplanting the induced mouse ESC-derived IPCs into immunodeficient mice in combination with mouse ESC-derived NPCs.[8] However, the study did not succeed in inducing mouse mesangial cells *in vitro*. Multi-lineage interactions among mesangial precursor cells, endothelial cells, and podocytes *in vivo* are crucial for mesangial-lineage development.[43] Here, we succeeded in inducing human mesangium-like cells in organoids by combining hiPSC-derived NPCs and IPLCs *in vitro* and mesangial-lineage cells *in vitro* by screening candidate inducing factors based on a transcriptional pathway analysis of HEK. Moreover, we found that the p38MAPK and hypoxia/VEGF pathways and SHH pathway contribute to the development of mesangial-lineage and EPO-producing cells, respectively, by analyzing the induced cells. High-glucose conditions activate p38 MAPK signaling in mesangial cells,[83–85] and phosphorylated ERK(+) and p38 MAPK(+) cells in glomeruli and renal interstitial cells are increased in patients with diabetic nephropathy.[86] Mesangial cells proliferate in diabetic nephropathy,[14] which is possibly relevant to our findings of mesangial-lineage induction *in vitro*.

Multi-cellular kidney organoids consisting of podocytes, proximal and distal tubular cells, stromal cells, and endothelial cells treated with a cyclic AMP activator, forskolin, produce RENIN.[72] This observation is consistent with our scRNA-seq analysis of developing human kidneys in which cyclic AMP-mediated signaling was detected in stromal cells differentiating to RENIN(+) mesangial lineages (Item S4).

In mice, Epo production first occurs in neural crest or neuroepithelium and then in liver, but at around birth, kidneys take over the production.[12] EPO-producing cells in kidney are considered of Foxd1(+) IPC origin, which is different from EPO-producing cells in liver.[13] EPO-producing cells in kidney regulate erythropoiesis in adults but also play roles in kidney fibrosis in chronic kidney disease (CKD).[24,87] Therefore, the induction of renal EPO-producing cells may have value for elucidating the mechanisms of kidney fibrosis in CKD. Previous reports that differentiated EPO-producing cells from hiPSCs modified the differentiation method of liver[88] and neural crest,[89] but the generation of hiPSC-derived EPO-producing cells of kidney lineages has not been reported.

The developmental process of renal EPO-producing cells has been the subject of several labeling systems.[24,87,90,91] However, little is known about their differentiation signals. Although kidney is not the main site of Epo production during the embryonic period,[92] postnatal anemia increases the number of Epo-producing cells in kidneys even on postnatal day 5.[91] Therefore, an Epo-producing subpopulation of Foxd1(+) IPC-derived stromal cells may be present during the embryonic period and either increase in number or continue maturing after birth. Our IPLCs produce EPO upon the modulation of specific signaling pathways, including the SHH signal, suggesting a link to their developmental signals *in vivo*. Therefore, further comparative studies of hiPSC-derived

Figure 6. Molecular events during transition from IPCs to mesangial lineages

(A) Pseudotime trajectory analysis of clusters for stromal progenitors and cortical stroma cells (C0), cortical and medullary stroma cells (C2), and cortical stroma and mesangial cells (C5).

(B) Heatmap of DEGs during the transition from C0 to C2 or C5 following the trajectory timeline. Activated canonical pathways predicted by IPA based on each clustered DEG (left) and DEGs clustered by their expression patterns (right).

(C) RT-qPCR analysis of markers for JG (*RENIN* and *GJA4*) and mesangial cells (*EBF1*, *GJA5*, *ITGA8*, and *GATA3*) and *VEGFA* after treatment in hypoxic (CFR+B7+SB in 5% O_2) or normoxic (CFR+B7+SB minus FG-4592 in 20% O_2) condition with or without VEGF (100 ng/mL) or axitinib (3 μM) on days 11–15. Data are presented as the mean ± SEM, and dots indicate independent experimental data using 17K6 cells (n = 4 or 8).

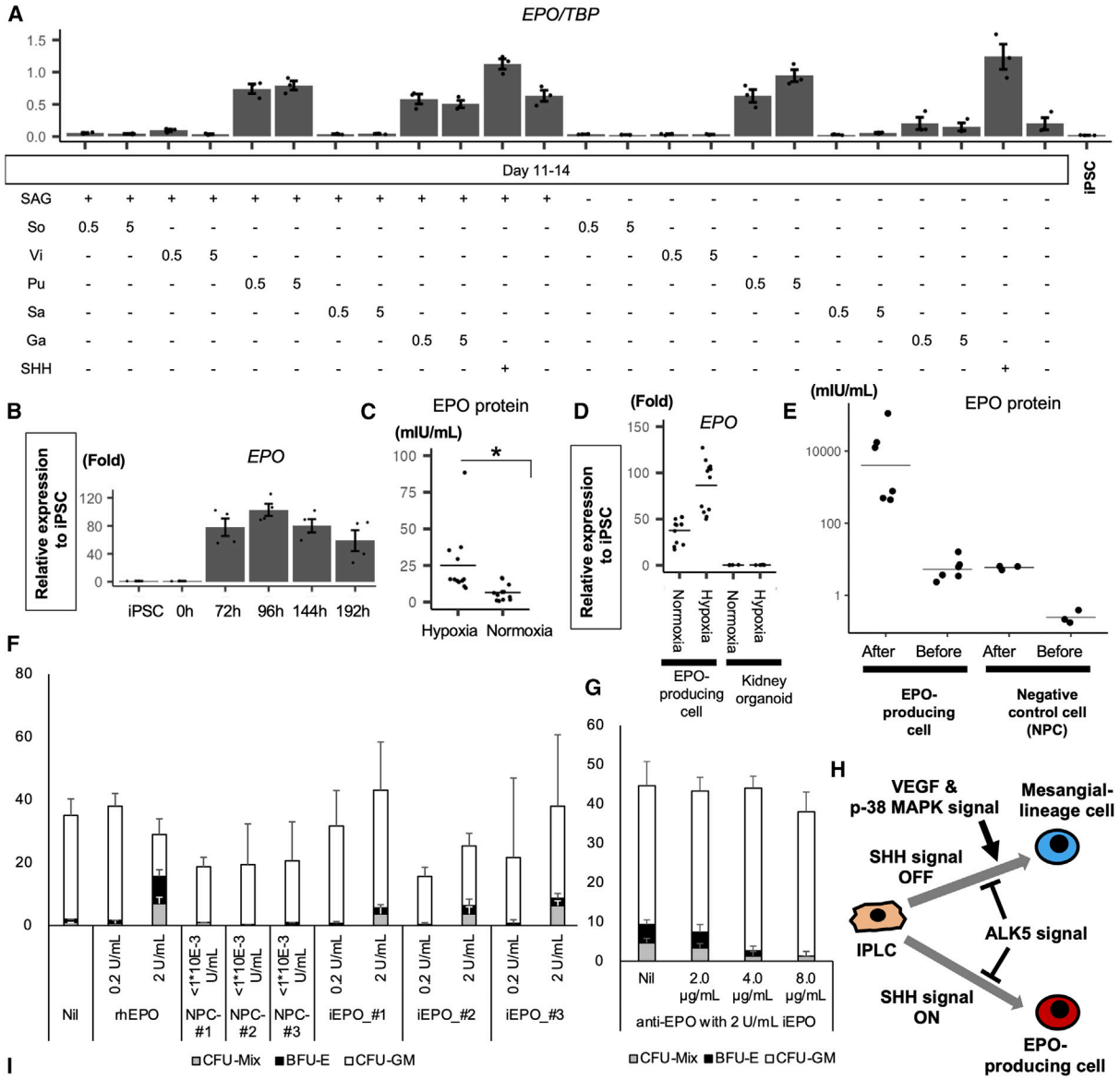

I

Mesoderm specification	Posterior IM-committing PS					PSM induction	IPLC induction	Mesangial-lineage cell
						SI+S		CFR+B7+SB+V
1 d	1 d	1 d	1 d	freeze	2 d	2 d	3 d	3-8 d
5 μM CHIR99021 10 nM RA 1 ng/mL BMP4 100 ng/mL FGF2	5 μM CHIR99021 100 ng/mL FGF2 1 ng/mL BMP7	5 μM CHIR99021 10 μM A83-01 (1 ng/mL BMP7 or 100 nM LDN193189)	5 μM CHIR99021 30 ng/mL FGF2 10 ng/mL Activin A 30 μM Y-27632	Can be cryopreserved (optional)	5 μM CHIR99021 30 ng/mL FGF2 10 ng/mL Activin A 30 μM Y-27632	1 μM CHIR99021 500 nM SAG 10 μM SB431542 10 ng/mL IL-1β 0.1 μM RA	1 μM CHIR99021 500 nM SAG 10 μM SB431542 0.1 μM RA	1 μM CHIR99021 10 μM SB431542 0.1 μM RA (10 μM FG-4592) 100 ng/mL BMP7 100 ng/mL VEGF
Mesoderm specification	**Posterior IM-committing PS**					**PSM induction**	**IPLC induction**	**EPO-producing cell**
						SI+S		**CFR+A83+SHH**
1 d	1 d	1 d	1 d	freeze	2 d	2 d	3 d	3-8 d under 5%O_2
5 μM CHIR99021 10 nM RA 1 ng/mL BMP4 100 ng/mL FGF2	5 μM CHIR99021 100 ng/mL FGF2 1 ng/mL BMP7	5 μM CHIR99021 10 μM A83-01 (1 ng/mL BMP7 or 100 nM LDN193189)	5 μM CHIR99021 30 ng/mL FGF2 10 ng/mL Activin A 30 μM Y-27632	Can be cryopreserved (optional)	5 μM CHIR99021 30 ng/mL FGF2 10 ng/mL Activin A 30 μM Y-27632	1 μM CHIR99021 500 nM SAG 10 μM SB431542 10 ng/mL IL-1β 0.1 μM RA	1 μM CHIR99021 500 nM SAG 10 μM SB431542 0.1 μM RA	1 μM CHIR99021 1 μM A83-01 0.1 μM RA 10 μM FG-4592 100 ng/mL SHH

(legend on next page)

EPO-producing cells and EPO-producing cells during development are warranted.

Interestingly, a previous lineage-tracing study showed T(+) PPS cells at E9.5 do not commit to MM[9]; however, our scRNA-seq analysis showed the pseudotime developmental trajectory of T(+) E9.5 PPS to PSM and IPCs. We suspect three possible explanations for this discrepancy. First, we sampled five embryos each at E9.5 and E10.5 and pooled them at each stage. However, these embryos may have some degree of variation in the developmental stage, and T(+) cells in relatively less advanced embryos are committed to kidney even at E9.5. Second, the previous study[9] had a time lag between the application of tamoxifen and Cre-recombinase activation. Third, because of the transcriptional continuity of PPS, IM, and PSM in the current embryo-level resolution analysis, the lineage may appear developmentally continuous in the pseudotemporal analysis.

In conclusion, we developed a selective renal IPLC-induction method from hiPSCs that can generate mesangial and EPO-producing cell lineages and revealed crucial roles of p38 MAPK signaling in mesangial-lineage development (Figures 7H and 7I). Our IPC-lineage differentiation system will contribute to kidney regeneration and developmental research.

Limitations of the study

Unlike a previous report using mice,[8,10] we did not succeed in forming kidney tissues with higher-order structures from hiPSC-derived NPCs, IPLCs, and NDCs. We hypothesized that higher-order structures could not be achieved because our IPLCs cannot undergo proper physiological interactions. A landmark report in this field suggested that different co-culture conditions between humans and mice may be the underlying cause.[10] It is difficult to experimentally validate this hypothesis because we cannot easily access HEK nor isolate viable IPCs from HEK tissues. However, using an available public HEK dataset, we confirmed that our IPLCs approach each stromal subset of HEK tissues when combined with hiPSC-derived NPCs and NDCs and formed kidney organoids. Finally, regardless of morphology, our IPLCs are not considered functionally inferior because they formed cap mesenchyme-like structures and differentiated into mesangial-lineage and EPO-producing cells. Therefore, future studies should modify culture conditions and differentiation protocols based on more analysis of developing kidneys and improve organoid technologies to enable NPC-, IPC-, and UB-derived kidney tissue reconstruction *in vitro*. We co-cultured EGFP(+)IPLCs and non-fluorescent NPCs and examined whether the mesangial structures were EGFP labeled. However, glomerular EGFP and PDGFRB expressions did not completely merge, likely because EGFP is expressed in the cytoplasm by CAG promoter-driven transgenes in the AAVS1 locus,[44] whereas PDGFRB is expressed on the cell surface. Nevertheless, IPLCs derived from EGFP-expressing hiPSCs integrate with glomeruli as PDGFRB-positive cells.

STAR★METHODS

Detailed methods are provided in the online version of this paper and include the following:

- KEY RESOURCES TABLE
- RESOURCE AVAILABILITY
  - Lead contact
  - Materials availability
  - Data and code availability
- EXPERIMENT MODEL AND STUDY PARTICIPANT DETAILS
  - Human tissues
  - Mice
  - Cynomolgus monkey
  - hiPSC Maintenance
- METHOD DETAILS
  - Differentiation protocols
  - Cryopreservation of NPCs
  - Thawing cryopreserved NPCs
  - Kidney reconstruction *In vitro*
  - Organ culture
  - Generation of OSR1-GFP/FOXD1-tdTomato reporter hiPSC line
  - Whole Mount immunostaining
  - Section immunostaining
  - Flow cytometry and cell sorting
  - RT-PCR and Real-time quantitative RT-PCR (RT-qPCR)
  - Genomic Real-time quantitative PCR

Figure 7. SHH signal agonists induce *EPO* expression

(A) RT-qPCR analysis of *EPO* expression to compare the effects of SHH signaling modulators in CFR+A83 medium on days 11–14 of the differentiation protocol.
(B) RT-qPCR analysis of temporal *EPO* expression after CFR+A83+SHH treatment.
(C) Quantification of EPO protein in culture medium of IPLCs after treatment with CFR+A83+SHH under 5% O_2 and with CFR+A83+SHH minus FG-4592 under 20% O_2.
(D) RT-qPCR analysis of *EPO* expression to compare the effects of oxygenic conditions on IPLCs treated with CFR+A83+SHH (EPO-producing cells) and NPC-derived kidney organoids.[17]
(E) Quantification of EPO protein in culture medium of EPO-producing cells and NPCs treated with CFR+A83+SHH under 5% O_2 before and after 30 kDa ultrafiltration.
(F and G) Number of clonal colonies on a semisolid medium containing SCF, GM-CSF, IL-3, IL-6, and G-CSF supplemented with rhEPO or iEPO (F) or iEPO and anti-EPO neutralizing antibodies (G).
(H) Summary of the signals elucidated in this study.
(I) Outline of the directed differentiation protocols established in this study.
Data are presented as the mean ± SEM using 201B7 cells (n = 3) in (F) and (G). Dots indicate independent experimental data using 17K6 cells (n = 3 in A and n = 4–6 in B). Dots and lines in the center of the scatterplots indicate experimental data and mean values, respectively, from four independent experiments and three technical replicates in (C), 4–12 independent experiments in (D), and three independent experiments and two technical replicates in (E) using 201B7 cells. SAG, 500 nM and SHH, 100 ng/mL. So, sonidegib; Vi, vismodegib; Pu, purmophamine; Sa, SANT-1; Ga, GANT61. The units of So, Vi, Pu, Sa, and Ga are μM in (A).

- Protein assay
- Proximity immunoassay for EPO protein quantification
- Clonogenic hematopoietic progenitor assay
- Single-cell RNA-seq
- Bulk RNA-seq

- QUANTIFICATION AND STATISTICAL ANALYSIS
  - Single-cell RNA-seq data processing
  - Bulk RNA-seq data processing
  - Image quantification of marker Protein(+) cells
  - Statistical analysis

SUPPLEMENTAL INFORMATION

Supplemental information can be found online at https://doi.org/10.1016/j.celrep.2023.113602.

ACKNOWLEDGMENTS

The authors would like to thank Dr. Peter Karagiannis for critically reading and revising the manuscript, Drs. Masaki Nomura, Akito Tanaka, Leif Wigge, and Gustav Holmgren for helpful discussion and technical support, Drs. Naohide Ageyama, Tomoyuki Tsukiyama, Naoya Toriu, Motoko Yanagita, Hideaki Tsuchiya, and Chizuru Iwatani for the management and support of experiments using cynomolgus monkey kidneys, and Dr. Kiyotoshi Sekiguchi for providing various laminin fragments. This research is supported by RegeNephro Co., Ltd., by AstraZeneca plc, by AMED (JP23bm1123002, JP22bm0104001, JP22bm0804013, and JP22bk0104113) to K. Osafune, and by the iPS Cell Research Fund.

AUTHOR CONTRIBUTIONS

Project administration, H.T.; supervision, M.K.S., M.S., T.Y., C.G., K.J.W., and K. Osafune; conceptualization and methodology, H.T. and K. Osafune; investigation, H.T., A.H., S.-I.M., T.A., W.C., Y.I., M.N.-K., S.S., K. Okita, K.M., and A.N.; formal analysis, H.T., M.K.S., M.S., T.Y., C.G., K.J.W., and K. Osafune; writing – original draft, H.T.; writing – review & editing, H.T., A.H., S.-I.M., T.A., W.C., Y.I., M.N.-K., S.S., K. Okita, K.M., A.N., M.K.S., M.S., T.Y., C.G., K.J.W., and K. Osafune.

DECLARATION OF INTERESTS

K. Osafune is a founder and member of the scientific advisory boards of iPS Portal and a founder and chief scientific advisor of RegeNephro Co., Ltd. H.T. is an employee of RegeNephro Co., Ltd. S.-I.M. is a scientific advisor of RegeNephro Co., Ltd. T.A. is a founder and scientific advisor of RegeNephro Co., Ltd. C.G. and K.J.W. are employees of AstraZeneca plc. H.T. and K. Osafune have a patent pending for a method for producing the renal interstitial-lineage cells described in this study.

Received: May 11, 2022
Revised: June 13, 2023
Accepted: December 5, 2023
Published: January 17, 2024

REFERENCES

1. Little, M.H., and McMahon, A.P. (2012). Mammalian Kidney Development: Principles, Progress, and Projections. Cold Spring Harb. Perspect. Biol. *4*, a008300.
2. Islam, M., and Nishinakamura, R. (2019). How to Rebuild the Kidney: Recent Advances in Kidney Organoids (Preprint at Oxford University Press (OUP).
3. Kobayashi, A., Valerius, M.T., Mugford, J.W., Carroll, T.J., Self, M., Oliver, G., and McMahon, A.P. (2008). Six2 Defines and Regulates a Multipotent Self-Renewing Nephron Progenitor Population throughout Mammalian Kidney Development. Cell Stem Cell *3*, 169–181.
4. Yu, J., Carroll, T.J., and McMahon, A.P. (2002). Sonic hedgehog regulates proliferation and differentiation of mesenchymal cells in the mouse metanephric kidney. Development *129*, 5301–5312.
5. Humphreys, B.D., Lin, S.L., Kobayashi, A., Hudson, T.E., Nowlin, B.T., Bonventre, J.V., Valerius, M.T., McMahon, A.P., and Duffield, J.S. (2010). Fate tracing reveals the pericyte and not epithelial origin of myofibroblasts in kidney fibrosis. Am. J. Pathol. *176*, 85–97.
6. Mugford, J.W., Yu, J., Kobayashi, A., and McMahon, A.P. (2009). High-resolution gene expression analysis of the developing mouse kidney defines novel cellular compartments within the nephron progenitor population. Dev. Biol. *333*, 312–323.
7. Mugford, J.W., Sipilä, P., McMahon, J.A., and McMahon, A.P. (2008). Osr1 expression demarcates a multi-potent population of intermediate mesoderm that undergoes progressive restriction to an Osr1-dependent nephron progenitor compartment within the mammalian kidney. Dev. Biol. *324*, 88–98.
8. Tanigawa, S., Tanaka, E., Miike, K., Ohmori, T., Inoue, D., Cai, C.-L., Taguchi, A., Kobayashi, A., and Nishinakamura, R. (2022). Generation of the organotypic kidney structure by integrating pluripotent stem cell-derived renal stroma. Nat. Commun. *13*, 611.
9. Taguchi, A., Kaku, Y., Ohmori, T., Sharmin, S., Ogawa, M., Sasaki, H., and Nishinakamura, R. (2014). Redefining the in vivo origin of metanephric nephron progenitors enables generation of complex kidney structures from pluripotent stem cells. Cell Stem Cell *14*, 53–67.
10. Taguchi, A., and Nishinakamura, R. (2017). Higher-Order Kidney Organogenesis from Pluripotent Stem Cells. Cell Stem Cell *21*, 730–746.e6.
11. England, A.R., Chaney, C.P., Das, A., Patel, M., Malewska, A., Armendariz, D., Hon, G.C., Strand, D.W., Drake, K.A., and Carroll, T.J. (2020). Identification and characterization of cellular heterogeneity within the developing renal interstitium. Development *147*.
12. Suzuki, N. (2015). Erythropoietin gene expression: Developmental-stage specificity, cell-type specificity, and hypoxia inducibility. Tohoku J. Exp. Med. *235*, 233–240.
13. Kobayashi, H., Liu, Q., Binns, T.C., Urrutia, A.A., Davidoff, O., Kapitsinou, P.P., Pfaff, A.S., Olauson, H., Wernerson, A., Fogo, A.B., et al. (2016). Distinct subpopulations of FOXD1 stroma-derived cells regulate renal erythropoietin. J. Clin. Invest. *126*, 1926–1938.
14. Steffes, M.W., Osterby, R., Chavers, B., and Mauer, S.M. (1989). Mesangial expansion as a central mechanism for loss of kidney function in diabetic patients. Preprint *38*, 1077–1081.
15. Takasato, M., Er, P.X., Chiu, H.S., Maier, B., Baillie, G.J., Ferguson, C., Parton, R.G., Wolvetang, E.J., Roost, M.S., Chuva de Sousa Lopes, S.M., and Little, M.H. (2015). Kidney organoids from human iPS cells contain multiple lineages and model human nephrogenesis. Nature *526*, 564–568.
16. Uchimura, K., Wu, H., Yoshimura, Y., and Humphreys, B.D. (2020). Human Pluripotent Stem Cell-Derived Kidney Organoids with Improved Collecting Duct Maturation and Injury Modeling. Cell Rep. *33*, 108514.
17. Tsujimoto, H., Kasahara, T., Sueta, S.I., Araoka, T., Sakamoto, S., Okada, C., Mae, S.I., Nakajima, T., Okamoto, N., Taura, D., et al. (2020). A Modular Differentiation System Maps Multiple Human Kidney Lineages from Pluripotent Stem Cells. Cell Rep. *31*, 107476.
18. Takasato, M., Er, P.X., Chiu, H.S., and Little, M.H. (2016). Generation of kidney organoids from human pluripotent stem cells. Nat. Protoc. *11*, 1681–1692.
19. Morizane, R., and Bonventre, J.V. (2017). Generation of nephron progenitor cells and kidney organoids from human pluripotent stem cells. Nat. Protoc. *12*, 195–207.
20. Miyazaki, T., Isobe, T., Nakatsuji, N., and Suemori, H. (2017). Efficient Adhesion Culture of Human Pluripotent Stem Cells Using Laminin Fragments in an Uncoated Manner. Sci. Rep. *7*, 41165.

21. Takayama, K., Akita, N., Mimura, N., Akahira, R., Taniguchi, Y., Ikeda, M., Sakurai, F., Ohara, O., Morio, T., Sekiguchi, K., and Mizuguchi, H. (2017). Generation of safe and therapeutically effective human induced pluripotent stem cell-derived hepatocyte-like cells for regenerative medicine. Hepatol. Commun. *1*, 1058–1069.

22. Mae, S.-I., Shono, A., Shiota, F., Yasuno, T., Kajiwara, M., Gotoda-Nishimura, N., Arai, S., Sato-Otubo, A., Toyoda, T., Takahashi, K., et al. (2013). Monitoring and robust induction of nephrogenic intermediate mesoderm from human pluripotent stem cells. Nat. Commun. *4*, 1367.

23. Toyohara, T., Mae, S.-I., Sueta, S.-I., Inoue, T., Yamagishi, Y., Kawamoto, T., Kasahara, T., Hoshina, A., Toyoda, T., Tanaka, H., et al. (2015). Cell Therapy Using Human Induced Pluripotent Stem Cell-Derived Renal Progenitors Ameliorates Acute Kidney Injury in Mice. Stem Cells Transl. Med. *4*, 980–992.

24. Asada, N., Takase, M., Nakamura, J., Oguchi, A., Asada, M., Suzuki, N., Yamamura, K.i., Nagoshi, N., Shibata, S., Rao, T.N., et al. (2011). Dysfunction of fibroblasts of extrarenal origin underlies renal fibrosis and renal anemia in mice. J. Clin. Invest. *121*, 3981–3990.

25. Itäranta, P., Viiri, K., Kaartinen, V., and Vainio, S. (2009). Lumbo-sacral neural crest derivatives fate mapped with the aid of Wnt-1 promoter integrate but are not essential to kidney development. Differentiation. *77*, 199–208.

26. Kamiya, D., Takenaka-Ninagawa, N., Motoike, S., Kajiya, M., Akaboshi, T., Zhao, C., Shibata, M., Senda, S., Toyooka, Y., Sakurai, H., et al. (2020). Induction of Functional Mesenchymal Stem/Stromal Cells from Human iPCs Via a Neural Crest Cell Lineage Under Xeno-Free Conditions. SSRN Journal.

27. Lindström, N.O., Guo, J., Kim, A.D., Tran, T., Guo, Q., De Sena Brandine, G., Ransick, A., Parvez, R.K., Thornton, M.E., Basking, L., et al. (2018). Conserved and Divergent Features of Mesenchymal Progenitor Cell Types within the Cortical Nephrogenic Niche of the Human and Mouse Kidney. J. Am. Soc. Nephrol.

28. Hernández-García, D., Fuentes-Jiménez, D., Rojo-León, V., Wood, C., García, C., and Covarrubias, L. (2019). Hedgehog signaling dynamics in mouse embryos determined by a bioluminiscent reporter. Int. J. Dev. Biol. *63*, 605–613.

29. Platt, K.A., Michaud, J., and Joyner, A.L. (1997). Expression of the mouse Gli and Ptc genes is adjacent to embryonic sources of hedgehog signals suggesting a conservation of pathways between flies and mice. Mech. Dev. *62*, 121–135.

30. McDermott, A., Gustafsson, M., Elsam, T., Hui, C.C., Emerson, C.P., and Borycki, A.G. (2005). Gli2 and Gli3 have redundant and context-dependent function in skeletal muscle formation. Development *132*, 345–357.

31. Rowan, C.J., Li, W., Martirosyan, H., Erwood, S., Hu, D., Kim, Y.K., Sheybani-Deloui, S., Mulder, J., Blake, J., Chen, L., and Rosenblum, N.D. (2018). Hedgehog-GLI signaling in Foxd1- positive stromal cells promotes murine nephrogenesis via TGF β signaling. Development *145*, dev159947.

32. Becht, E., McInnes, L., Healy, J., Dutertre, C.-A., Kwok, I.W.H., Ng, L.G., Ginhoux, F., and Newell, E.W. (2018). Dimensionality reduction for visualizing single-cell data using UMAP. Nat. Biotechnol. *37*, 38–44.

33. He, P., Williams, B.A., Trout, D., Marinov, G.K., Amrhein, H., Berghella, L., Goh, S.-T., Plajzer-Frick, I., Afzal, V., Pennacchio, L.A., et al. (2020). The changing mouse embryo transcriptome at whole tissue and single-cell resolution. Nature *583*, 760–767.

34. Lau, Y.-F.C. (2020). Y chromosome in health and diseases. Cell Biosci. *10*, 97.

35. Cerase, A., Young, A.N., Ruiz, N.B., Buness, A., Sant, G.M., Arnold, M., Di Giacomo, M., Ascolani, M., Kumar, M., Hierholzer, A., et al. (2021). Chd8 regulates X chromosome inactivation in mouse through fine-tuning control of Xist expression. Commun. Biol. *4*, 485.

36. Zhou, Y., Zhou, B., Pache, L., Chang, M., Khodabakhshi, A.H., Tanaseichuk, O., Benner, C., and Chanda, S.K. (2019). Metascape provides a biologist-oriented resource for the analysis of systems-level datasets. Nat. Commun. *10*, 1523.

37. Guillaume, R., Bressan, M., and Herzlinger, D. (2009). Paraxial mesoderm contributes stromal cells to the developing kidney. Dev. Biol. *329*, 169–175.

38. Subramanian, A., Tamayo, P., Mootha, V.K., Mukherjee, S., Ebert, B.L., Gillette, M.A., Paulovich, A., Pomeroy, S.L., Golub, T.R., Lander, E.S., and Mesirov, J.P. (2005). Gene set enrichment analysis: A knowledge-based approach for interpreting genome-wide expression profiles. Proc. Natl. Acad. Sci. USA *102*, 15545–15550.

39. Menon, R., Otto, E.A., Kokoruda, A., Zhou, J., Zhang, Z., Yoon, E., Chen, Y.-C., Troyanskaya, O., Spence, J.R., Kretzler, M., and Cebrián, C. (2018). Single-cell analysis of progenitor cell dynamics and lineage specification in the human fetal kidney. Development *145*, dev164038.

40. Umekage, M., Sato, Y., and Takasu, N. (2019). Overview: an iPS cell stock at CiRA. Inflamm. Regen. *39*, 17.

41. Costantini, F., and Kopan, R. (2010). Patterning a complex organ: Branching morphogenesis and nephron segmentation in kidney development. Dev. Cell *18*, 698–712.

42. Mae, S.I., Ryosaka, M., Sakamoto, S., Matsuse, K., Nozaki, A., Igami, M., Kabai, R., Watanabe, A., and Osafune, K. (2020). Expansion of Human iPSC-Derived Ureteric Bud Organoids with Repeated Branching Potential. Cell Rep. *32*, 107963.

43. Vaughan, M.R., and Quaggin, S.E. (2008). How do mesangial and endothelial cells form the glomerular tuft? Preprint *19*, 24–33.

44. Oceguera-Yanez, F., Kim, S.I., Matsumoto, T., Tan, G.W., Xiang, L., Hatani, T., Kondo, T., Ikeya, M., Yoshida, Y., Inoue, H., and Woltjen, K. (2016). Engineering the AAVS1 locus for consistent and scalable transgene expression in human iPSCs and their differentiated derivatives. Methods *101*, 43–55.

45. He, B., Chen, P., Zambrano, S., Dabaghie, D., Hu, Y., Möller-Hackbarth, K., Unnersjö-Jess, D., Korkut, G.G., Charrin, E., Jeansson, M., et al. (2021). Single-cell RNA sequencing reveals the mesangial identity and species diversity of glomerular cell transcriptomes. Nat. Commun. *12*, 2141.

46. Holloway, E.M., Wu, J.H., Czerwinski, M., Sweet, C.W., Wu, A., Tsai, Y.-H., Huang, S., Stoddard, A.E., Capeling, M.M., Glass, I., and Spence, J.R. (2020). Differentiation of Human Intestinal Organoids with Endogenous Vascular Endothelial Cells. Dev. Cell *54*, 516–528.e7.

47. Bohnenpoll, T., Bettenhausen, E., Weiss, A.C., Foik, A.B., Trowe, M.O., Blank, P., Airik, R., and Kispert, A. (2013). Tbx18 expression demarcates multipotent precursor populations in the developing urogenital system but is exclusively required within the ureteric mesenchymal lineage to suppress a renal stromal fate. Dev. Biol. *380*, 25–36.

48. Wilson, S.B., Howden, S.E., Vanslambrouck, J.M., Dorison, A., Alquicira-Hernandez, J., Powell, J.E., and Little, M.H. (2022). DevKidCC allows for robust classification and direct comparisons of kidney organoid datasets. Genome Med. *14*, 19.

49. Katagiri, N., Hitomi, H., Mae, S.I., Kotaka, M., Lei, L., Yamamoto, T., Nishiyama, A., and Osafune, K. (2021). Retinoic acid regulates erythropoietin production cooperatively with hypoxia-inducible factors in human iPSC-derived erythropoietin-producing cells. Sci. Rep. *11*, 3936–4012.

50. Blank, U., Seto, M.L., Adams, D.C., Wojchowski, D.M., Karolak, M.J., and Oxburgh, L. (2008). An in vivo reporter of BMP signaling in organogenesis reveals targets in the developing kidney. BMC Dev. Biol. *8*. 86-18.

51. Miyazaki, Y., Oshima, K., Fogo, A., Hogan, B.L., and Ichikawa, I. (2000). Bone morphogenetic protein 4 regulates the budding site and elongation of the mouse ureter. J. Clin. Invest. *105*, 863–873.

52. Dudley, A.T., Lyons, K.M., and Robertson, E.J. (1995). A requirement for bone morphogenetic protein-7 during development of the mammalian kidney and eye. Genes Dev. *9*, 2795–2807.

53. Green, M.C. (1968). Mechanism of the pleiotropic effects of the short-ear mutant gene in the mouse. J. Exp. Zool. *167*, 129–150.

54. Dudley, A.T., and Robertson, E.J. (1997). Overlapping expression domains of bone morphogenetic protein family members potentially account for limited tissue defects in BMP7 deficient embryos. Dev. Dynam. *208*, 349–362.

55. Boyle, S.C., Liu, Z., and Kopan, R. (2014). Notch signaling is required for the formation of mesangial cells from a stromal mesenchyme precursor during kidney development. Development (Camb.) *141*, 346–354.

56. Grigorieva, I.V., Oszwald, A., Grigorieva, E.F., Schachner, H., Neudert, B., Ostendorf, T., Floege, J., Lindenmeyer, M.T., Cohen, C.D., Panzer, U., et al. (2019). A novel role for GATA3 in mesangial cells in glomerular development and injury. J. Am. Soc. Nephrol. *30*, 1641–1658.

57. Gerl, K., Steppan, D., Fuchs, M., Wagner, C., Willam, C., Kurtz, A., and Kurt, B. (2017). Activation of Hypoxia Signaling in Stromal Progenitors Impairs Kidney Development. Am. J. Pathol. *187*, 1496–1511.

58. Shi, Y., and Massagué, J. (2003). Mechanisms of TGF-Signaling from Cell Membrane to the Nucleus. Cell *113*, 685–700.

59. Patel, S.R., and Dressler, G.R. (2005). BMP7 signaling in renal development and disease. Trends Mol. Med. *11*, 512–518.

60. Derynck, R., and Zhang, Y.E. (2003). Smad-dependent and Smad-independent pathways in TGF-β family signalling. Nature *425*, 577–584.

61. Awazu, M., Omori, S., and Hida, M. (2002). MAP kinase in renal development. Nephrol. Dial. Transplant. *17*, 5–7.

62. Lindström, N.O., Sealfon, R., Chen, X., Parvez, R.K., Ransick, A., De Sena Brandine, G., Guo, J., Hill, B., Tran, T., Kim, A.D., et al. (2021). Spatial transcriptional mapping of the human nephrogenic program. Dev. Cell *56*, 2381–2398.e6.

63. Sequeira Lopez, M.L.S., and Gomez, R.A. (2011). Development of the renal arterioles. J. Am. Soc. Nephrol. *22*, 2156–2165.

64. Chung, J.J., Goldstein, L., Chen, Y.J.J., Lee, J., Webster, J.D., Roose-Girma, M., Paudyal, S.C., Modrusan, Z., Dey, A., and Shaw, A.S. (2020). Single-cell transcriptome profiling of the kidney glomerulus identifies key cell types and reactions to injury. J. Am. Soc. Nephrol. *31*, 2341–2354.

65. Mukhopadhyay, D., Tsiokas, L., Zhou, X.M., Foster, D., Brugge, J.S., and Sukhatme, V.P. (1995). Hypoxic induction of human vascular endothelial growth factor expression through c-Src activation. Nature *375*, 577–581.

66. Briscoe, J., and Thérond, P.P. (2013). The mechanisms of Hedgehog signalling and its roles in development and disease. Nat. Rev. Mol. Cell Biol. *14*, 416–429.

67. Lauth, M., Bergström, A., Shimokawa, T., and Toftgård, R. (2007). Inhibition of GLI-mediated transcription and tumor cell growth by small-molecule antagonists. Proc. Natl. Acad. Sci. USA *104*, 8455–8460.

68. Koning, M., Dumas, S.J., Avramut, M.C., Koning, R.I., Meta, E., Lievers, E., Wiersma, L.E., Borri, M., Liang, X., Xie, L., et al. (2022). Vasculogenesis in kidney organoids upon transplantation. NPJ Regen. Med. *7*, 40.

69. Lawlor, K.T., Vanslambrouck, J.M., Higgins, J.W., Chambon, A., Bishard, K., Arndt, D., Er, P.X., Wilson, S.B., Howden, S.E., Tan, K.S., et al. (2021). Cellular extrusion bioprinting improves kidney organoid reproducibility and conformation. Nat. Mater. *20*, 260–271.

70. Vanslambrouck, J.M., Wilson, S.B., Tan, K.S., Groenewegen, E., Rudraraju, R., Neil, J., Lawlor, K.T., Mah, S., Scurr, M., Howden, S.E., et al. (2022). Enhanced metanephric specification to functional proximal tubule enables toxicity screening and infectious disease modelling in kidney organoids. Nat. Commun. *13*, 5943.

71. Howden, S.E., Wilson, S.B., Groenewegen, E., Starks, L., Forbes, T.A., Tan, K.S., Vanslambrouck, J.M., Holloway, E.M., Chen, Y.H., Jain, S., et al. (2021). Plasticity of distal nephron epithelia from human kidney organoids enables the induction of ureteric tip and stalk. Cell Stem Cell *28*, 671–684.e6.

72. Shankar, A.S., Du, Z., Mora, H.T., van den Bosch, T.P.P., Korevaar, S.S., Van den Berg-Garrelds, I.M., Bindels, E., Lopez-Iglesias, C., Clahsen-van Groningen, M.C., Gribnau, J., et al. (2021). Human kidney organoids produce functional renin. Kidney Int. *99*, 134–147.

73. Lemos, D.R., McMurdo, M., Karaca, G., Wilflingseder, J., Leaf, I.A., Gupta, N., Miyoshi, T., Susa, K., Johnson, B.G., Soliman, K., et al. (2018). Interleukin-1b activates a MYC-dependent metabolic switch in kidney stromal cells necessary for progressive tubulointerstitial fibrosis. J. Am. Soc. Nephrol. *29*, 1690–1705.

74. Quintero-Ronderos, P., and Laissue, P. (2018). The multisystemic functions of FOXD1 in development and disease. J. Mol. Med. *96*, 725–739.

75. Boivin, F.J., and Bridgewater, D. (2018). β-Catenin in stromal progenitors controls medullary stromal development. Am. J. Physiol. Renal Physiol. *314*, F1177–F1187.

76. Guillot, C., Djeffal, Y., Michaut, A., Rabe, B., and Pourquié, O. (2021). Dynamics of primitive streak regression controls the fate of neuromesodermal progenitors in the chicken embryo. Elife *10*, e64819.

77. Rivera-Pérez, J.A., and Magnuson, T. (2005). Primitive streak formation in mice is preceded by localized activation of Brachyury and Wnt3. Dev. Biol. *288*, 363–371.

78. Takasato, M., Er, P.X., Becroft, M., Vanslambrouck, J.M., Stanley, E.G., Elefanty, A.G., and Little, M.H. (2014). Directing human embryonic stem cell differentiation towards a renal lineage generates a self-organizing kidney. Nat. Cell Biol. *16*, 118–126.

79. Hayashi, S., Suzuki, H., and Takemoto, T. (2021). The nephric mesenchyme lineage of intermediate mesoderm is derived from Tbx6-expressing derivatives of neuro-mesodermal progenitors via BMP-dependent Osr1 function. Dev. Biol. *478*, 155–162.

80. Dias, A., Lozovska, A., Wymeersch, F.J., Nóvoa, A., Binagui-Casas, A., Sobral, D., Martins, G.G., Wilson, V., and Mallo, M. (2020). A Tgfbr1/Snai1-dependent developmental module at the core of vertebrate axial elongation. Elife *9*, e56615–e56628.

81. Mugford, J.W., Sipilä, P., Kobayashi, A., Behringer, R.R., and McMahon, A.P. (2008). Hoxd11 specifies a program of metanephric kidney development within the intermediate mesoderm of the mouse embryo. Dev. Biol. *319*, 396–405.

82. Dunwoodie, S.L., Rodriguez, T.A., and Beddington, R.S. (1998). Msg1 and Mrg1, founding members of a gene family, show distinct patterns of gene expression during mouse embryogenesis. Mech. Dev. *72*, 27–40.

83. Wilmer, W.A., Dixon, C.L., and Hebert, C. (2001). Chronic exposure of human mesangial cells to high glucose environments activates the p38 MAPK pathway. Kidney Int. *60*, 858–871.

84. Haneda, M., Koya, D., Isono, M., and Kikkawa, R. (2003). Overview of Glucose Signaling in Mesangial Cells in Diabetic Nephropathy. J. Am. Soc. Nephrol. *14*, 1374–1382.

85. Haneda, M., Araki, S., Togawa, M., Sugimoto, T., Isono, M., and Kikkawa, R. (1997). Mitogen-activated protein kinase cascade is activated in glomeruli of diabetic rats and glomerular mesangial cells cultured under high glucose conditions. Diabetes *46*, 847–853.

86. Sakai, N., Wada, T., Furuichi, K., Iwata, Y., Yoshimoto, K., Kitagawa, K., Kokubo, S., Kobayashi, M., Hara, A., Yamahana, J., et al. (2005). Involvement of extracellular signal-regulated kinase and p38 in human diabetic nephropathy. Am. J. Kidney Dis. *45*, 54–65.

87. Souma, T., Yamazaki, S., Moriguchi, T., Suzuki, N., Hirano, I., Pan, X., Minegishi, N., Abe, M., Kiyomoto, H., Ito, S., and Yamamoto, M. (2013). Plasticity of Renal Erythropoietin-Producing Cells Governs Fibrosis. J. Am. Soc. Nephrol. *24*, 1599–1616.

88. Hitomi, H., Kasahara, T., Katagiri, N., Hoshina, A., Mae, S.I., Kotaka, M., Toyohara, T., Rahman, A., Nakano, D., Niwa, A., et al. (2017). Human pluripotent stem cell-derived erythropoietin-producing cells ameliorate renal anemia in mice. Sci. Transl. Med. *9*, eaaj2300.

89. Brizi, V., Buttò, S., Cerullo, D., Michele Lavecchia, A., Rodrigues-Diez, R., Novelli, R., Corna, D., Benigni, A., Remuzzi, G., and Xinaris, C. (2021). Human iPSC-derived neural crest stem cells can produce EPO and induce erythropoiesis in anemic mice. Stem Cell Res. *55*, 102476.

90. Kaneko, K., Sato, Y., Uchino, E., Toriu, N., Shigeta, M., Kiyonari, H., Endo, S., Fukuma, S., and Yanagita, M. (2022). Lineage tracing analysis defines erythropoietin-producing cells as a distinct subpopulation of resident fibroblasts with unique behaviors. Kidney Int. *102*, 280–292.

91. Pan, X., Suzuki, N., Hirano, I., Yamazaki, S., Minegishi, N., and Yamamoto, M. (2011). Isolation and Characterization of Renal Erythropoietin-Producing Cells from Genetically Produced Anemia Mice. PLoS One *6*, e25839.

92. Suzuki, N., Obara, N., Pan, X., Watanabe, M., Jishage, K.-I., Minegishi, N., and Yamamoto, M. (2011). Specific Contribution of the Erythropoietin Gene 3′ Enhancer to Hepatic Erythropoiesis after Late Embryonic Stages. Mol. Cell Biol. *31*, 3896–3905.

93. Yamasaki, J., Iwatani, C., Tsuchiya, H., Okahara, J., Sankai, T., and Torii, R. (2011). Vitrification and transfer of cynomolgus monkey (Macaca fascicularis) embryos fertilized by intracytoplasmic sperm injection. Theriogenology *76*, 33–38.

94. Sasaki, K., Oguchi, A., Cheng, K., Murakawa, Y., Okamoto, I., Ohta, H., Yabuta, Y., Iwatani, C., Tsuchiya, H., Yamamoto, T., et al. (2021). The embryonic ontogeny of the gonadal somatic cells in mice and monkeys. Cell Rep. *35*, 109075.

95. Nakagawa, M., Taniguchi, Y., Senda, S., Takizawa, N., Ichisaka, T., Asano, K., Morizane, A., Doi, D., Takahashi, J., Nishizawa, M., et al. (2014). A novel efficient feeder-Free culture system for the derivation of human induced pluripotent stem cells. Sci. Rep. *4*, 3594.

96. Watanabe, K., Ueno, M., Kamiya, D., Nishiyama, A., Matsumura, M., Wataya, T., Takahashi, J.B., Nishikawa, S., Nishikawa, S.i., Muguruma, K., and Sasai, Y. (2007). A ROCK inhibitor permits survival of dissociated human embryonic stem cells. Nat. Biotechnol. *25*, 681–686.

97. Zhao, M., Sekiguchi, K., and Sakurai, H. (2017). NEW GENERATION MATRIX PROVIDES HIGH EFFICIENT DIFFERENTIATION SYSTEM INDUCING MYOCYTES AND MUSCLE STEM CELLS FROM HUMAN INDUCED PLURIPOTENT STEM CELLS. In ISSCR Annual Meeting, p. 139.

98. Mae, S.-I., Ryosaka, M., Toyoda, T., Matsuse, K., Oshima, Y., Tsujimoto, H., Okumura, S., Shibasaki, A., and Osafune, K. (2018). Generation of branching ureteric bud tissues from human pluripotent stem cells. Biochem. Biophys. Res. Commun. *495*, 954–961.

99. Shi, M., McCracken, K.W., Patel, A.B., Zhang, W., Ester, L., Valerius, M.T., and Bonventre, J.V. (2023). Human ureteric bud organoids recapitulate branching morphogenesis and differentiate into functional collecting duct cell types. Nat. Biotechnol. *41*, 252–261.

100. Tsujimoto, H., Araoka, T., Nishi, Y., Ohta, A., Nakahata, T., and Osafune, K. (2021). Small molecule TCS21311 can replace BMP7 and facilitate cell proliferation in in vitro expansion culture of nephron progenitor cells. Biochem. Biophys. Res. Commun. *558*, 231–238.

101. Chen, J.Q., Heldman, M.R., Herrmann, M.A., Kedei, N., Woo, W., Blumberg, P.M., and Goldsmith, P.K. (2013). Absolute quantitation of endogenous proteins with precision and accuracy using a capillary Western system. Anal. Biochem. *442*, 97–103.

102. Greenwood, C., Ruff, D., Kirvell, S., Johnson, G., Dhillon, H.S., and Bustin, S.A. (2015). Proximity assays for sensitive quantification of proteins. Biomol. Detect. Quantif. *4*, 10–16.

103. Umeda, K., Heike, T., Nakata-Hizume, M., Niwa, A., Arai, M., Shinoda, G., Ma, F., Suemori, H., Luo, H.Y., Chui, D.H.K., et al. (2006). Sequential Analysis of α- and β-Globin Gene Expression During Erythropoietic Differentiation from Primate Embryonic Stem Cells. Stem Cell. *24*, 2627–2636.

104. Satija, R., Farrell, J.A., Gennert, D., Schier, A.F., and Regev, A. (2015). Spatial reconstruction of single-cell gene expression data. Nat. Biotechnol. *33*, 495–502.

105. Hao, Y., Hao, S., Andersen-Nissen, E., Mauck, W.M., Zheng, S., Butler, A., Lee, M.J., Wilk, A.J., Darby, C., Zager, M., et al. (2021). Integrated analysis of multimodal single-cell data. Cell *184*, 3573–3587.e29.

106. Choudhary, S., and Satija, R. (2022). Comparison and evaluation of statistical error models for scRNA-seq. Genome Biol. *23*, 27.

107. Nestorowa, S., Hamey, F.K., Pijuan Sala, B., Diamanti, E., Shepherd, M., Laurenti, E., Wilson, N.K., Kent, D.G., and Göttgens, B. (2016). A single-cell resolution map of mouse hematopoietic stem and progenitor cell differentiation. Blood *128*, e20–e31.

108. Qiu, X., Hill, A., Packer, J., Lin, D., Ma, Y.A., and Trapnell, C. (2017). Single-cell mRNA quantification and differential analysis with Census. Nat. Methods *14*, 309–315.

109. Patro, R., Duggal, G., Love, M.I., Irizarry, R.A., and Kingsford, C. (2017). Salmon provides fast and bias-aware quantification of transcript expression. Nat. Methods *14*, 417–419.

110. Love, M.I., Huber, W., and Anders, S. (2014). Moderated estimation of fold change and dispersion for RNA-seq data with DESeq2. Genome Biol. *15*, 550.

111. Srivastava, A., Malik, L., Sarkar, H., Zakeri, M., Almodaresi, F., Soneson, C., Love, M.I., Kingsford, C., and Patro, R. (2020). Alignment and mapping methodology influence transcript abundance estimation. Genome Biol. *21*, 239.

STAR★METHODS

KEY RESOURCES TABLE

REAGENT or RESOURCE	SOURCE	IDENTIFIER
Antibodies		
BRACHYURY (T)	R&D	CAT. # AF2085; RRID:AB_2200235
CALB1	Synaptic systems	CAT. # 214-004; RRID:AB_10550535
DESMIN	Abcam	CAT. # ab32362; RRID:AB_731901
EPO	R&D	CAT. # AB-286-NA; RRID:AB_354338
FOXD1	Abcam	CAT. # ab129324; RRID:AB_11150609
GATA3	Cell Signaling	CAT. # 5852S; RRID:AB_10835690
GATA3	R&D	CAT. # AF2605; RRID:AB_2108571
GFP	Nacalai tesque	CAT. # 04404-84; RRID:AB_10013361
HOXC10	Abcam	CAT. # ab153904; RRID:AB_2687827
MAFB	Santa Cruz	CAT. # sc-74521; RRID:AB_1125981
MEIS1/2/3	Active Motif	CAT. # 39795; RRID:AB_2750570
NPHS1	PROGEN	CAT. # GP-N2; RRID:AB_1542487
HNF-4α	R&D	CAT. # MAB4605; RRID: AB_3076456
PBX1	Cell Signaling	CAT. # 4342; RRID:AB_2160295
PDGFRB	Proteintech	CAT. # 13449-1-AP RRID:AB_2162644
p-38 MAPK	Cell Signaling	CAT. # 8690S; RRID:AB_10999090
Phosphor-p38 MAPK	Cell Signaling	CAT. # 9215S; RRID:AB_331762
POU3F3 (BRN1)	Novus Biologicals	CAT. # NBP2-57011; RRID:AB_3065278
RENIN	Abcam	CAT. # ab212197; RRID:AB_2909418
RET	R&D	CAT. # AF1485; RRID:AB_35482
TBX6	R&D	CAT. # AF4744; RRID:AB_2200834
tdTomato (dsRed)	Clontech	CAT. # 632496; RRID:AB_10013483
Alexa Fluor 546 Donkey Anti-Mouse IgG (H + L)	Thermo Fisher Scientific	CAT. # A10036; RRID:AB_2534012
Alexa Fluor 488 Donkey Anti-Rabbit IgG (H + L)	Thermo Fisher Scientific	CAT. # A21206; RRID:AB_2535792
Alexa Fluor 488 Donkey Anti-Rat IgG (H + L)	Thermo Fisher Scientific	CAT. # A21208; RRID:AB_2535794
Alexa Fluor 546 Donkey Anti-Goat IgG (H + L)	Thermo Fisher Scientific	CAT. # A11056; RRID:AB_2534103
Alexa Fluor Plus 555 Donkey Anti-Goat IgG (H + L)	Thermo Fisher Scientific	CAT. # A32816; RRID:AB_2762839
Alexa Fluor Plus 555 Donkey Anti-Rabbit IgG (H + L)	Thermo Fisher Scientific	CAT. # A32794; RRID:AB_2762834
CF 555 Donkey Anti-Guinea Pig IgG (H + L)	Sigma-Aldrich	CAT. # SAB4600297; RRID: AB_2814810
Alexa Fluor 647 Donkey Anti-Guinea Pig IgG (H + L)	Jackson ImmunoResearch	CAT. # 706-605-148; RRID:AB_2340476
Alexa Fluor 647 Donkey Anti-Mouse IgG (H + L)	Thermo Fisher Scientific	CAT. # A31571; RRID:AB_162542
Alexa Fluor 647 Donkey Anti-Rabbit IgG (H + L)	Thermo Fisher Scientific	CAT. # A31573; RRID:AB_2536183
Alexa Fluor 647 Donkey Anti-Rat IgG (H + L)	Jackson ImmunoResearch	CAT. # 712-605-150; RRID:AB_2340693
Chemicals, peptides, and recombinant proteins		
Accumax	Innovative Cell Technologies	CAT. # AM105
Accutase	Nacalai tesque	CAT. # 12679-54
A83-01	Wako	CAT. # 018-26742
Afamin/Wnt3a CM	MBL	CAT. # J-ORMW301R
Axitinib	Selleck	CAT. #S1005
Beta-estradiol	Wako	CAT. # 056-04044
Blocker Casein in PBS	Thermo Fisher Scientific	CAT. # 37528

(*Continued on next page*)

Continued

REAGENT or RESOURCE	SOURCE	IDENTIFIER
BMP-4	Peprotech	CAT. # AF-120-05ET
BMP-5	R&D	CAT. # 615-BMC-020
BMP-7	R&D	CAT. # 354-BP
B-27 Supplement minus vitamin A	Thermo Fisher Scientific	CAT. # 12587001
CHIR99021	Wako	CAT. # 038-25443
DAPT	R&D	CAT. # 2634/10
DMEM/F-12, GlutaMAX	Thermo Fisher Scientific	CAT. # 10565042
Donkey Serum	Merck	CAT. #S30-100ML
Erythropoietin, Recombinant, Human	Merck	CAT. # 329871
Essential 6 Medium	Thermo Fisher Scientific	CAT. # A1516401
Estradiol	Wako	CAT. # 056-04044
FG-4592	Selleck	CAT. #S1007
GANT61	Selleck	CAT. #S8075
GDNF, Recombinant, Human	R&D	CAT. # 212-GD
Hoechst 33342	Invitrogen	CAT. #H3570
Human DLL4	R&D	CAT. # 1506-D4
Human FGF acidic	R&D	CAT. # 232-FA
Human FGF basic	Wako	CAT. # 060-04543
Human/Murine FGF-8b (FGF8)	Peprotech	CAT. # 100-25
Human FGF9	Peprotech	CAT. # 100-23
Human Sonic Hedgehog	R&D	CAT. # 1845-SH-100
iMatrix-511 silk	Nippi	CAT. # 892021
iMatrix-511	Nippi	CAT. # 892012
iMatrix-511MG	Nippi	CAT. # iMatrix-511MG
Interleukin 1β (IL-1β)	Wako	CAT. # 095-04611
Jagged1 Fc chimera	R&D	CAT. # 1277-JG-50
LDN193189	Axon Medchem	CAT. # Axon1509
Matrigel	BD	CAT. # 354230
MethoCult GF + semisolid medium without EPO	STEMCELL Technologies	CAT. #H4535
NOGGIN	Peprotech	CAT. # 120-10C
Normal donkey serum	Merk	CAT. # 566460
Penicillin-Streptomycin	Thermo Fisher Scientific	CAT. # 15140122
Phosphatase Inhibitor Cocktail SolutionI	Wako	CAT. # 167-24381
Protease Inhibitor Cocktail Set III DMSO Solution (EDTA free)	Wako	CAT. # 163-26061
Purmorphamine	Selleck	CAT. #S3042
Retinoic Acid	Sigma-Aldrich	CAT. #R2625
RIPA Buffer	Wako	CAT. # 182-02451
R-spondin 1	R&D	CAT. # 4645-RS-250
SB 431542	Nacalai tesque	CAT. # 18176-54
SB 203580	Wako	CAT. # 199-16551
Smoothened Agonist (SAG)	Selleck	CAT. #S7779
Sonidegib	Selleck	CAT. #S2151
STEM-CELLBANKER GMP grade	ZNQ	CAT. # CB047
Stem Fit AK02N	Takara Bio	CAT. # AK02N
TGF-β1	Peprotech	CAT. # AF-100-21C
TrypLE Select Enzyme	Thermo Fisher Scientific	CAT. # A1285901

(*Continued on next page*)

Continued

REAGENT or RESOURCE	SOURCE	IDENTIFIER
TTNPB	Santa Cruz	CAT. # sc-203303
VEGF 165	Peprotech	CAT. # 100-20
Vismodegib	Selleck	CAT. #S1082
Y-27632	Wako	CAT. # 257-00614
Critical commercial assays		
Amicon Ultra-15, PLTK Ultracell-30, 30kDa	Merk	CAT. # UFC903024
Anti-Rabbit Detection Module for Jess, Wes, Peggy Sue or Sally Sue	Protein Simple	CAT. # DM-001
CD34 Microbeads Kit, Human	Miltenyi Biotec	CAT. # 130-046-702
Chromium Next GEM Single Cell 3′ Kit v3.1	10X Genomics	CAT. # 1000269
ProQuantum Human EPO Immunoassay Kit	Themo Fisher Scientific	CAT. # A40419
ReverTra Ace	TOYOBO	CAT. # TRT-101
RNase-Free DNase Set	QIAGEN	CAT. # 79254
RNeasy Mini kit	QIAGEN	CAT. # 74106
SMARTer Stranded RNA-Seq Kit	Clontech	CAT. # 634839
SureSelect Strand Specific RNA Library Kit	Agilent	CAT. #G9691B
TB Green Premix Ex Taq (Tli RNaseH plus) ROX plus	Takara Bio	CAT. # RR42WR
Wes Separation Module for 12–230 kDa	Protein Simple	CAT. # SM-W002
XL-Bradford assay	Apro Science	CAT. # KY-1040
NovaSeq 6000 S1 Reagent Kit v1.5 (100cycle)	illumina	CAT. # 20028319
NovaSeq 6000 S2 Reagent Kit v1.5 (100cycle)	illumina	CAT. # 20028316
NovaSeq 6000 SP Reagent Kit v1.5 (100cycle)	illumina	CAT. # 20028401
NovaSeq 6000 SP Reagent Kit v1.5 (200cycle)	illumina	CAT. # 20040719
NextSeq 1000/2000 P2 Reagents (100cycle)	illumina	CAT. # 20046811
Deposited data		
Ensembl Archive Release 105 (Dec 2021)	EMBL-EBI	Release 105 (Dec 2021)
Homo sapiens GRCh38.p13	Ensembl	GRCh38.p13
Homo sapiens GRCh37.p13	Ensembl	GRCh37.p13
Human embryonic kidney cortex cells (GW14) single cell RNA-seq data	Lindström et al., 2021	GSE139280
Human embryonic kidney tissue from 2 individual biological specimens (GW13.7 and GW15.4)	Holloway et al., 2020	E-MTAB-9083
RNA sequencing data	This paper	DRA013763, DRA016361
Single cell RNA-Seq profiling of E9.5 and E10.5 mouse embryo (posterior parts)	This paper	DRA013676
Single cell RNA-Seq profiling of hiPSC-derived IPLCs	This paper	DRA017219
Single cell RNA-Seq profiling of kidney organoids generated from hiPSC-derived IPLCs, NPCs and NDCs	This paper	DRA017219
The pre-built Cell Ranger reference package: Mouse reference, mm10 (GENCODE vM23/Ensembl 98)	10X Genomics	References - 2020-A (July 7, 2020)
The pre-built Cell Ranger reference package: Mouse reference, GRCh38 (GENCODE v23/Ensembl 98)	10X Genomics	References - 2020-A (July 7, 2020)
Experimental models: Cell lines (biological sex)		
585A1 (male)	ICSCB	Stem cell ID: SKIP000858
201B7 (female)	ICSCB	Stem cell ID: SKIP000001
1231A3 (female)	ICSCB	Stem cell ID: HPS0381
1383D2 (male)	ICSCB	Stem cell ID: HPS1005
1383D6 (male)	ICSCB	Stem cell ID: HPS1006
4A6 (4A6C3-10) (female)	Toyohara et al., 2015	N/A
17K6 (female)	This paper	N/A

(*Continued on next page*)

Continued

REAGENT or RESOURCE	SOURCE	IDENTIFIER
317-12 (female)	Oceguera-Yanez et al., 2016	N/A
3D45 (female)	Mae et al., 2013	N/A
Ff-I 14s04 (male)	Umekage et al., 2019	N/A
Experimental models: Organisms/strains		
C57BL/6JJmsSlc	SHIMIZU Laboratory Supplies Co., Ltd	Jackson Laboratory: Stock No: 000664
NOD.Cg-*Prkdc*^{scid}*Il2rg*^{tm1Wjl}/SzJ	SHIMIZU Laboratory Supplies Co., Ltd	Jackson Laboratory: Stock No: 005557
Slc:ICR	SHIMIZU Laboratory Supplies Co., Ltd	Jackson Laboratory: Stock No: 009122
Oligonucleotides		
Primers for Figures 1, 3, 5–7, S1, and S3–S5 see Table S2	This paper	N/A
Software and algorithms		
biomaRt	EMBL-EBI	biomaRt_2.50.3
BZ-X Analyzer	KEYENCE	BZX700 or BZX800
Cell Ranger pipeline	10X Genomics	Cell Ranger version 5.0.0 or 6.1.2
DESeq2	Love et al., 2014	DESeq2_1.34.0
DevKidCC	Wilson et al., 2022	DevKidCC version 0.2.3 or 0.3.0
FACS Diva	BD	FACSDiva v8.0.1 Software
ImageJ2 (Fiji) 2.30/1.53f	Schneider et al., 2012	RRID:SCR_002285
Microsoft Excel for Mac	https://products.office.com/	Microsoft Office Standard 2013
Monocle2	Qiu et al., 2017	monocle_version 2.20.0
R	The R Foundation	R version 4.1.0. or 4.2.1.
RStudio	RStudio, Inc.	RStudio version 1.4.1717
Salmon	Patro et al., 2017	Salmon version 1.9.0
Seurat	Hao et al., 2021	Seurat version 4.0.4
ZEN 2 blue edition	ZEISS	ZEN 2.3 (blue edition)

RESOURCE AVAILABILITY

Lead contact

Further information and requests for resources and reagents should be directed to and will be fulfilled by the lead contact, K. Osafune (osafu@cira.kyoto-u.ac.jp).

Materials availability

This study did not generate new unique reagents. The OSR1-GFP/FOXD1-tdTomato double knock-in hiPSC (17K6) line generated in this study is available from the lead contact with a completed materials transfer agreement.

Data and code availability

- The RNA-seq data and the scRNA-seq data reported in this study are available from the corresponding author (KO) upon reasonable request. DNA DataBank of Japan accession numbers for the bulk RNA-seq data and the scRNA-seq data are DRA013763 and DRA016361, and DRA013676, respectively. The log2(scaledTPM+1) gene expression values from Salmon in Figure 1E are available in Item S5-1E, the TPM gene expression values of all IPLC samples in Figure S3D are available in Item S5-S3D, and the scaled TPM gene expression values of all samples in Figure S7F are available in Item S5-S7F. The output matrix data from the Cell Ranger count function is available in the Genomic Expression Archive (accession numbers: E-GEAD-494 and E-GEAD-657).
- This paper dose not report original code.
- Any additional information required to reanalyze the data reported in this paper is available from the lead contact upon reasonable request.

EXPERIMENT MODEL AND STUDY PARTICIPANT DETAILS

Human tissues

The human embryonic kidney cDNA used in Figure S3E is a pooled sample of 59 GW20-33 embryonic kidneys purchased from TaKaRa Bio. Informed consent for the use of CD34(+) hematopoietic progenitor cells was obtained from cord blood donors in accordance with the declaration of Helsinki and approved by the Ethics Committee of Kyoto University.

Mice

The Kyoto University Animal Care Committee approved all animal experiments. No formal randomization was performed in this study. C57BL/6 or ICR mice that were 9–10 days pregnant were purchased from SHIMIZU Laboratory Supplies Co., Ltd, Inc. All mice were housed at the animal facility of the Center for iPS Cell Research and Application (CiRA), Kyoto University, under specific pathogen-free conditions. The room had controlled temperature (21°C–25°C), humidity (45–55%) and light (12-h light-dark cycle). Mice were provided *ad libitum* access to food and water.[72]

Cynomolgus monkey

Procedures using cynomolgus monkeys were approved by the Animal Care and Use Committee of the Shiga University of Medical Science. The series of assisted reproductive technologies using cynomolgus monkeys, including oocyte collection, intra-cytoplasmic sperm injection, pre-implantation embryo culture and transfer of pre-implantation embryos into foster mothers, were done as reported previously.[93,94] The light cycle was 12 h of artificial light from 8 a.m. to 8 p.m. Water was available *ad libitum*. Temperature and humidity in the animal rooms were maintained at 23°C–27°C and 45–55%, respectively. Implanted embryos were scanned with transabdominal ultrasound monitoring and recovered by cesarean section under full anesthesia. Two E57 embryos were harvested in this study. The foster mothers were maintained after surgery.

hiPSC Maintenance

Experiments using hiPSCs were approved by the Ethics Committee of Kyoto University, and informed consent was obtained from donors from whom hiPSCs were derived. hiPSCs were maintained with feeder-free cultures using Stem Fit AK02N (Ajinomoto) supplemented with iMatrix-511 silk (Nippi), iMatrix-511 (Nippi) or iMatrix-511MG (Nippi).[20] The cells were passaged using a 1:1 mixture of TrypLE Select Enzyme (Thermo Fisher Scientific) and 0.5 mM EDTA/PBS (Thermo Fisher Scientific) every 4–5 days.[95] We added 10 μM Y-27632 (Wako) to AK02N only on the day (around 24 h) when we passaged the cells because it improves the survival of dissociated hPSCs.[96] hiPSCs were routinely examined for mycoplasma contamination.

METHOD DETAILS

Differentiation protocols

Posterior primitive streak (PPS) induction

hiPSCs were first treated using an enzymatic method with a 1:1 mixture of TrypLE Select Enzyme and 0.5 mM EDTA/PBS for 5 min and washed with PBS(−). The cells were then detached using a cell scraper, dissociated into single cells by gentle pipetting and seeded onto 24-well plates (Corning) at a density of 1.3 × 10^4 cells/cm^2 with 0.5 mL of Stem Fit AK02N supplemented with 10 μM Y-27632 and 2.4 μL/mL iMatrix-511 one day before the start of differentiation. After 24 h (day 0), the cells were cultured with serum-free differentiation medium consisting of DMEM/F12 Glutamax (Thermo Fisher Scientific), B27 supplement minus vitamin A (Thermo Fisher Scientific) and 0.5×Penicillin/streptomycin (hereafter called basal medium) supplemented with 1 or 5 μM CHIR99021 (Wako), 10 nM RA (Sigma), 1 ng/mL BMP4 (Peprotech) and 100 ng/mL bFGF (Wako). After another 24 h (day 1), the cells were cultured with basal medium containing 5 μM CHIR99021, 100 ng/mL bFGF and 1 ng/mL BMP7 (R&D Systems). On day 2, the medium was switched to basal medium containing 5 μM CHIR99021, 1 ng/mL BMP7 and 10 μM A83-01 (Wako). On day 3, the medium was changed to basal medium containing 5 μM CHIR99021, 30 ng/mL bFGF, 10 ng/mL activin A (R&D Systems) and 30 μM Y-27632 (Wako). On day 4, the cells were washed with PBS(−), treated with Accumax (Innovative Cell Technologies), dissociated into single cells by gentle pipetting, seeded on 24-well plates (CORNING) at a density of 1.05 × 10^5 cells/cm^2 (2D culture) or on 96-well low cell attachment plates (Thermo Fisher Scientific) at a density of 2.0 × 10^4 cells/well (3D culture) with basal medium containing 5 μM CHIR99021, 30 ng/mL bFGF, 10 ng/mL activin A, 30 μM Y-27632 and 1.2 μL/well iMatrix-511 or a laminin-E8 fragments library[97] (only for 2D culture) and cultured for 48 h.

For the hiPSC lines 1231A3, 1383D6, 1383D2, 201B7 and 317-12, we replaced BMP7 with 100 nM LDN-193189 in day 2 medium. We skipped the day 1 step (5 μM CHIR99021, 100 ng/mL FGF2 and 1 ng/mL BMP7) for 1231A3.

Posterior intermediate mesoderm (IM) and metanephric NPC induction

On day 6 of the PPS induction, the medium was changed to basal medium containing 0.1 μM RA and 25 ng/mL NOGGIN (Peprotech). On day 8, the medium was switched to basal medium containing 200 ng/mL FGF9 and 1 μM CHIR99021, and the cells were incubated for 72 h.

3D differentiation protocols using stirring bioreactor

On day 4, the cells were washed with PBS(−), treated with Accumax, dissociated into single cells by gentle pipetting, seeded at a density of 3.0 × 10^6 cells/vessel (able, BWV-S03A) with 30 mL of basal medium containing 5 μM CHIR99021, 30 ng/mL bFGF, 10 ng/mL activin A and 30 μM Y-27632 and cultured for 48 h. On day 6, the cells were cultured in basal medium containing 0.1 μM RA, 25 ng/mL NOGGIN and 200 ng/mL FGF9. On day 8, the medium was switched to basal medium containing 200 ng/mL FGF9 and 1 μM CHIR99021, and the cells were incubated for 72 h. The agitation speed was 40 rpm.

Interstitial progenitor-like cell (IPLC) induction

On day 4 of the PPS induction, the dissociated cells, either after or without cryopreservation using STEM-CELLBANKER (ZNQ), were seeded on 96-well U-bottom plates (Sumitomo Bakelite or Thermo Fisher Scientific) at a density of 1.0-2.0 × 10^4 cells/well with basal medium containing 5 μM CHIR99021, 30 ng/mL bFGF, 10 ng/mL activin A and 30 μM Y-27632 to form cellular aggregates and cultured for 48 h.

On day 6, the cells were incubated with AK02N minus bFGF medium (Ajinomoto) or basal medium containing 1 μM CHIR99021, 0.1 μM RA, 500 nM smoothened agonist (SAG) (Selleck), 10 μM SB431542 (Nakalai tesque) and 10 ng/mL IL-1α (Wako). On day 8, the cells were incubated with AK02N minus bFGF medium or basal medium containing 1 μM CHIR99021, 0.1 μM RA, 500 nM SAG and 10 μM SB431542 for 72 h.

Mesangial-lineage cell induction

On day 11, the cells were incubated with basal medium containing 1 μM CHIR99021, 0.1 μM RA, 10 μM FG-4592 (Selleck), 100 ng/mL BMP7, 10 μM SB431542 and 100 ng/mL VEGF for 72–192 h under hypoxic condition (5% O_2) or 1 μM CHIR99021, 0.1 μM RA, 100 ng/mL BMP7 (R&D Systems), 10 μM SB431542 (Nakalai tesque) and 100 ng/mL VEGF (Peprotech) for 72–192 h under normoxic condition.

EPO-expressing cell induction

On day 11, the cells were incubated with basal medium containing 1 μM CHIR99021, 0.1 μM RA, 10 μM FG-4592, 100 ng/mL hSHH (R&D Systems) and 1 μM A83-01 for 72–192 h under 5% O_2.

Anterior IM induction

hiPSCs were directed to ND lineages as described previously with some modification.[42,98,99] hiPSCs were first treated using an enzymatic method with a 1:1 mixture of TrypLE Select Enzyme and 0.5 mM EDTA/PBS for 5 min and washed with PBS(−). The cells were then detached using a cell scraper, dissociated into single cells by gentle pipetting and seeded onto a 10-cm dish (Falcon) at a density of 4.0 × 10^5 cells/dish with 10 mL of Stem Fit AK02N supplemented with 10 μM Y-27632 and 20 μL/dish iMatrix-511 one day before the start of the differentiation. After 24 h (day 0), the cells were cultured with serum-free differentiation medium consisting of Essential 6 medium (E6; Thermo Fisher Scientific) supplemented with 50 ng/mL activin A, 5 μM CHIR99021, 25 ng/mL BMP4 and 25 ng/mL bFGF. After around 22 h (day 1), the cells were cultured with E6 medium containing 100 nM LDN193189, 1 μM A83-01, 0.1 μM TTNPB (Santa Cruz Biotechnology) and 200 ng/mL FGF8 (Peprotech) for two days. Then the cells were replated at a density of 8.7 × 10^6 cells/dish on a 10-cm dish in E6 medium containing the same 4 factors and 10 μM Y- 27632 and incubated for an additional 24 h to induce anterior IM.

NDC induction

Anterior IM cells were treated with E6 medium containing 1 μM CHIR99021, 100 nM LDN193189, 200 ng/mL FGF8, 100 ng/mL GDNF and 0.1 μM TTNPB for 2 days and dissociated into single cells by pipetting after treatment with Accutase (Nacalai tesque) for 3 min at 37°C. Either after or without cryopreservation using STEM-CELLBANKER,[42] the cells were seeded onto low-attachment 96-well plates (Sumitomo Bakelite) at a density of 1.0 × 10^4 cells/well and treated with the same medium and factors plus 10 μM Y-27632 to induce NDC aggregates for 2 days.

Cryopreservation of NPCs

On day 10 of the NPC induction, the cells were dissociated into single cells by incubation with Accumax for 5 min at 37°C and gentle pipetting and spun down for 3 min at 200*g*, and the supernatant was removed. The cell pellet was gently resuspended in ice-cold STEM CELL BANKER at a density of 1.0 × 10^7 cells/mL. The tubes were placed into a pre-cooled BICELL (Nihon freezer), kept for 10–15 min at 4°C and then placed into a −80°C freezer. After 12–24 h, the tubes were transferred to liquid nitrogen tanks for long-term storage.

Thawing cryopreserved NPCs

The tubes were placed in a 37°C water bath until they were half-thawed. Then, ice-cold 0.7 mL PBS(−) supplemented with 10 μM Y-27632 and 10% v/v basal medium was immediately added into the tubes. After spinning down for 3 min at 200*g* and removing the supernatant, the cells were gently resuspended in ice-cold basal medium containing 200 ng/mL FGF9, 1 μM CHIR99021 and 10 μM Y-27632 at a live cell density of 1.0 × 10^6 cells/mL and seeded at 4.0 × 10^4 cells/well in low cell attachment 96-well U-bottom plates. After spinning down the plate for 3 min at 200*g*, the cells were incubated for 48–120 h at 37°C.

Kidney reconstruction *In vitro*

Cryopreserved and thawed NPC aggregates, day 11 IPLCs and NDCs were dissociated into single cells by incubation with Accumax for 10 min at 37°C and gentle pipetting. The dissociated single cells were mixed, resuspended in basal medium containing 1 μM

CHIR99021, 0.1 μM RA, 100 ng/mL FGF9 and 10 μM Y-27632 with or without the factors tested in Figures S4A and S4B and seeded into 96-well low cell-binding U-bottom plates at a density of 1.7 × 10^4 NPCs/well, 1.7 × 10^4 IPLCs/well and 1.7 × 10^4 NDCs/well to form aggregates. After 48 h, mixed aggregates were transferred to a 24-well plate and incubated at 37°C for 30 min with 20 μL of 50% Matrigel in the same medium described above. After solidification to some extent, 180 μL of the same medium was added. Then, the medium was replaced with half the volume of fresh basal medium every two days.

Organ culture

Isolated metanephros of E13.5 mice were transferred onto transwell inserts (Corning) and cultured with basal medium containing 1 μM CHIR99021, 10 μM FG-4592 and 0.1 μM RA with or without 100 ng/mL BMP7 and 10 μM SB431542 for 48 h at 37°C under 5% O_2.

Generation of OSR1-GFP/FOXD1-tdTomato reporter hiPSC line

We established OSR1-GFP/FOXD1-tdTomato double knock-in hiPSC lines using our previously reported gene targeting strategy.[22,23] We constructed the BAC-based vector shown in Figure 1B, in which a tdTomato reporter gene was knocked in to the FOXD1 locus. A part of the FOXD1 gene sequences we used to generate the reporter strains is shown in Item S1-FOXD1-genome, in which the sequences marked in yellow, green and blue are the sequence removed by homologous recombination, the homology arm shown in Figure 1B and the qPCR primer pair used for the strain selection, respectively. We selected the line 17K6 as a candidate homologous recombinant with heterozygous tdTomato reporter gene and normal karyotype from 57 drug-resistant clones, in which genomic qPCR analysis by TaqMan assays showed the mean relative quantity was 0.75 (n = 2) compared to the control OSR1-GFP/SIX2-tdTomato reporter hiPSC line with intact FOXD1 gene loci (4A6) derived from the same parental OSR1-GFP reporter hiPSC line (3D45) (Figure S1G).

Whole Mount immunostaining

The embryo samples were fixed with 4% PFA/PBS overnight at 4°C after a brief wash with PBS(−). The samples were then treated with CUBIC-L solution diluted with distilled water at a 1:1 ratio on a shaker for 24 h at 37°C for tissue clearing. The next day, the samples were treated with CUBIC-L solution on the shaker for 24–48 h at 37°C. After washing with PBS(−) for 6 h at 4°C three times, the samples were incubated with Blocker Casein overnight at 4°C. Primary antibodies were diluted with Blocker Casein and incubated with the samples on the shaker for 48 h at 4°C. After washing with PBS(−) for 6 h twice, the samples were incubated again with Blocker Casein overnight at 4°C. The samples were then incubated with secondary antibodies on the shaker for 48 h at 4°C. After washing with PBS(−) twice, the samples were treated with CUBIC-R+ solution diluted with distilled water at a 1:1 ratio on the shaker for 8 h at 4°C. Finally, the samples were treated with CUBIC-R+ solution on the shaker for 24 h at room temperature. Fluorescent images were captured using a confocal microscope (Zeiss LSM710 or Olympus FV3000). Image analysis was performed using ImageJ version 2.1.0/1.53c.

Section immunostaining

Day 11 IPLC aggregates were fixed with 4% PFA/PBS overnight at 4°C after a brief wash with PBS(−). The fixed cells were washed twice with PBS(−), treated with 30% w/w sucrose for 2 h at 4°C and embedded in OTC compound (Sakura Finetek Japan). The specimens were quickly frozen using liquid nitrogen. Then, 10-μm thick frozen sections were prepared using a cryostat (Leica). The sections were washed with distilled water and blocked with Blocker Casein in PBS(−) with or without normal donkey serum (Merck) for 30 min at 4°C. Primary antibodies were diluted in Blocker Casein in PBS(−) and incubated with the sections for 24 h at 4°C. After washing with PBS (−), the sections were blocked again with Blocker Casein in PBS(−) for 10 min at 4°C. Secondary antibodies and DAPI (Thermo Fisher Scientific) were incubated for 2 h at 4°C. The antibodies used in this study are listed in key resources table.

Fluorescent images were captured using a BZ-X700 or -X800 (KEYENCE) or confocal microscope (Zeiss LSM710 or Olympus FV3000). Image analysis was performed using a BZ-X Analyzer (KEYENCE) or ImageJ version 2.1.0/1.53c.

Flow cytometry and cell sorting

The cells were incubated with Accumax for 5 min at 37°C and dissociated by pipetting. Dead cells stained with DAPI were excluded from the analyses. The cells were analyzed and sorted using a FACS Aria II cell sorter (BD). The isolated cells were collected in basal medium containing 10 μM Y-27632. The data were analyzed using the FACS Diva (BD) software program. Non-fluorescent NPCs derived from hiPSC lines without gene modifications (201B7 or Ff-I 14s04) were used as a negative control. Gating was set such that DAPI(−) live cells had a positive fraction of less than 1% for the negative control cells.

RT-PCR and Real-time quantitative RT-PCR (RT-qPCR)

Total RNA was isolated using an RNeasy Kit (Qiagen) according to the manufacturer's recommendations, followed by cDNA synthesis using standard protocols. Briefly, the extracted RNA on the RNeasy Kit column was treated with DNase I (Qiagen) for 15 min, and the cDNA was synthesized using up to 1 μg of total RNA of each sample and ReverTra Ace (TOYOBO) on a Veriti Thermal Cycler (Applied Biosystems). qPCR was performed using QuantStudio 3 (Thermo Fisher Scientific) and TB Green Premix Ex Taq (Tli RNaseH plus) ROX plus (Takara) according to the manufacturer's recommendations. The primer sequences are listed in Table S2.

Genomic Real-time quantitative PCR

Real-time PCR reactions were carried out with 100 ng of genomic DNA, 250 nM of TaqMan probe and 500 nM of primers using standard protocols (Thermo Fisher Scientific). The sequences of the primers are listed in Table S2.

Protein assay

Cell aggregates were dissociated by pipetting in RIPA buffer (Wako) supplemented with an EDTA-free Protease Inhibitor Cocktail Set DMSO Solution (Wako) and Phosphatase Inhibitor Cocktail Solution (Wako) on ice and sonicated. The cell debris was removed by centrifugation for 20 min at 10,000*g*. The protein concentration was analyzed by the XL-Bradford assay (Apro Science) and measured using a PE Envision 2104 Mutilabel Reader (PerkinElmer). Protein measurements for p38 MAPK and phospho-p38 MAPK were performed as reported previously.[100] Briefly, using the cellular lysates, the protein expression was quantified by a capillary Western blot assay (Protein Simple).[101] Proteins (1.5 μg/sample) were separated through a size-resolving matrix in the capillaries, immobilized to the inner capillary wall and incubated with primary antibodies at a concentration of 1:50 in antibody dilution buffer (Protein Simple) and with anti-rabbit secondary antibodies (Protein Simple) before detection using chemiluminescence. Signals reflected as the area under the curve (AUC) of the target proteins were generated automatically at the end of each run. Phosphorylated protein levels were quantified as the ratio of the AUC from each sample that was normalized to the AUC of the corresponding total target protein. Prior to the AUC measurements, the linear dynamic range of the sample concentration was confirmed using linear regression analysis for each target protein. The calibration curves were prepared using lysates with a diluted series of hiPSC proteins. The measurement of Renin in the culture supernatant or Renin activity in ultrafiltration concentration was measured by LSI Medience Corporation. We removed cell debris from the culture supernatant of mesangial-lineage cell aggregates by centrifugation at 2,380*g* for 60 min at 4°C. Then, using 13 mL of the supernatant, Renin protein was concentrated using AmiconUltra-30 (MerckMillipore) by centrifugation at 2,380*g* for 60 min at room temperature.

Proximity immunoassay for EPO protein quantification

IPLCs were incubated in 0.6 mL of basal medium under EPO cell induction condition (1 μM CHIR99021, 0.1 μM RA, 10 μM FG-4592, 100 ng/mL hSHH and 1 μM A83-01) for 96 h and 5% O_2, and then culture supernatant was collected. We used basal medium as a blank control. The cell debris was removed by centrifugation for 20 min at 10,000*g* and the quantification of human EPO protein was performed using a ProQuantum Human EPO Immunoassay Kit (Thermo Fisher Scientific) following the kit protocol, which utilizes the principles of proximity ligation and amplification techniques to detect target antigens.[102] Two EPO protein-specific antibodies supplied in the kit are each bound to unique oligos. We allowed the antibodies to react with antigen in the culture supernatant diluted with the buffer supplied in the kit for 1 h at room temperature. When the two antibodies bind to their target sites, their oligos are designed to be close to each other, allowing ligation by the ligase supplied in the kit at 25°C for 20 min. Then, the oligos turn into the amplification target nucleotide sequence. The sequence was amplified and analyzed using QuantStudio 3 with the specific primer pair, TaqMan probe, and the PCR enzyme supplied in the kit. Quantification was performed by building a calibration curve using a dilution series of the EPO standard protein provided in the kit. The value measured in the blank sample was subtracted from each measured value to calculate the amount of EPO protein in the supernatant. The number of trypan blue (Nakalai tesque) negative cells in the aggregates at the time of the culture supernatant collection was measured using a TC20 Automated Cell Counter (Bio-Rad) to estimate the amount of EPO protein secretion per million live cells.

Clonogenic hematopoietic progenitor assay

Human CD34(+) cells were isolated from cord blood using antibody-conjugated beads enrichment (Miltenyi Biotec) following the manufacturer's instructions. A total of 5×10^5 CD34(+) cells were incubated with EPO protein from culture supernatant of hiPSC-derived EPO-producing cells (iEPO) or rhEPO (positive control) at 0.2 and 2 IU/mL or negative control culture supernatant of NPCs treated with EPO-producing cell induction condition (basal medium containing 1 μM CHIR99021, 0.1 μM RA, 10 μM FG-4592, 100 ng/mL hSHH and 1 μM A83-01 for 96 h under 5% O_2) for 2 h. We removed cell debris from the culture supernatant of hiPSC-derived EPO-producing cells or NPC aggregates by centrifugation at 2,380*g* for 60 min at 4°C. Then, using 13 mL of the supernatant, hiPSC-EPO protein was concentrated using AmiconUltra-30 (MerckMillipore) by centrifugation at 2,380*g* for 60 min at room temperature. Quantification of enriched EPO protein was performed using a proximity immunoassay as described above. CD34(+) cells were cultured in MethoCult GF + semisolid medium (1 mL/dish) (STEMCELL Technologies) containing stem cell factor (SCF), granulocyte macrophage colony stimulating factor (GM-CSF), IL-3, IL-6 and granulocyte colony-stimulating factor (G-CSF) supplemented with rEPO or iEPO at a low cell density. In the experiments to neutralize iEPO, 2 IU/mL iEPO and 0, 2, 4 or 8 μg/mL of anti-EPO antibody (R&D Systems) were supplemented. After 21 days of culture, colonies were counted, and colony types [CFU-Mix (mixed colony-forming units), BFU-E and CFU-GM] were determined by *in situ* observation using an inverted microscope according to previously described criteria.[88,103]

Single-cell RNA-seq

For mice, the posterior parts of E9.5 and E10.5 mouse embryos were manually dissected, treated with Accumax for 5 min at 37°C and dissociated by pipetting. Although we did not check the biological sex of the embryos, we assumed that the combined five samples at each stage analyzed were a mix of biological sexes based on a sex marker examination of single-cell RNA-seq samples (Figure S2C).

Dead cells stained with DAPI were excluded, and DAPI(−) cells were sorted using a FACS Aria II cell sorter. The isolated cells were collected in PBS(−) containing 0.04% BSA and 10 μM Y-27632 and centrifuged for 5 min at 200*g*. The cell pellet was resuspended in PBS(−) containing 0.04% BSA and 10 μM Y-27632. The live cell number was counted by trypan blue staining, and the library preparation was performed targeting 5,000 cells using a Chromium Single Cell 3′ Reagent Kit v3.1 (10X Genomics) and the Chromium Controller (10X Genomics) according to the manufacturer's instructions (CellPrepGuide CG000053; ChromiumNextGEMSingleCell3_v3.1 CG000204). After the cDNA synthesis, library amplification PCR was done using 12 cycles. The library was sequenced on a NextSeq 500/550 High Output Kit v2.5 with Read 1: 28 base pairs (bp), Index 1: 8 bp (Illumina i7 index) and Read 2: 91 bp.

For IPLCs and day-12 kidney organoids generated from hiPSC-derived IPLCs, NPCs and NDCs, cells were treated with Accumax for 10 min at 37°C and dissociated by pipetting. The cells were collected in PBS(−) containing 0.04% BSA and 10 μM Y-27632 and centrifuged for 3 min at 200*g*. The cell pellet was resuspended in PBS(−) containing 0.04% BSA and 10 μM Y-27632. The live cell number was counted by trypan blue staining, and the library preparation was performed targeting 5,000 cells using a Chromium Single Cell 3′ Reagent Kit v3.1and the Chromium Controller. After the cDNA synthesis, library amplification PCR was done using 12–13 cycles. The library was sequenced on a NovaSeq Reagent Kit v1.5 with Read 1: 28 base pairs (bp), Index 1: 10bp, Index 2: 10bp and Read 2: 90 bp.

Bulk RNA-seq

Total RNA was isolated using the RNeasy Mini Kit. The samples were preserved at −80°C, and the library preparation and sequencing for bulk RNA-seq were conducted by three different institutions (DNAFORM, the CiRA Foundation and Kyoto University), which resulted in several variations in the methods described below.

For the analysis shown in Figure 1E, after poly(A)(+) RNA enrichment using a NEBNext Poly(A) mRNA Magnetic Isolation Module (New England BioLabs), double-stranded cDNA libraries (RNA-seq libraries) were prepared using a SMARTer Stranded RNA-Seq Kit (Clontech) according to the manufacturer's instructions. The library was sequenced using the NextSeq 500/550 High Output Kit v2.5 (75 Cycles) with 50-8-8-25 cycles (Illumina). For the analysis shown in Figure S3D, we prepared sequencing libraries using TruSeq Stranded Total RNA (Illumina). The library was sequenced using the NovaSeq SP Reagent Kit v1.5 (200 cycles) with 101-8-8-101 cycles. For the analysis shown in Figure S7F, we prepared sequencing libraries using the SureSelect Strand-Specific RNA Library Prep System (Agilent). The library was sequenced using the NextSeq 500/550 v2.5 Kit (150 cycles) with 76-9-0-76 cycles.

QUANTIFICATION AND STATISTICAL ANALYSIS

Single-cell RNA-seq data processing

For mice, the deconvolution of unique molecular identifiers (UMIs) and cell barcodes of BCL files, alignment to the mouse reference genome GRCm38 (GENCODE vM23/Ensembl 98), and UMI counting were conducted using the Cell Ranger v5.0.0 pipeline (10X Genomics). To check the quality of the data and to remove multiplets, we performed Seurat-based[104] filtering based on three criteria: the number of detected features (nFeature_RNA) per cell, the number of UMIs expressed per cell (nCount_RNA) and the percentage of mitochondrial gene count (percent.mt) using the following threshold parameters: nFeature_RNA (2000–9000) and percentage of mitochondrial genes expressed (<10%).[105] We merged the filtered subset of raw count matrices and performed a standard NormalizeData, FindVariableFeatures, ScaleData workflow of Seurat for the downstream analysis.

hiPSC-derived IPLCs, day-12 kidney organoids generated from hiPSC-derived IPLCs, NPCs and NDCs, and the downloaded gestational day-96 and -108 human embryonic kidney tissue dataset (ArrayExpress: E-MTAB-9083) were compared as follows. The deconvolution of UMIs and cell barcodes of BCL files, alignment to the human reference genome GRCh38 (GENCODE v32/Ensembl 98), and UMI counting were conducted using the Cell Ranger v6.1.2 pipeline (10X Genomics). We performed Seurat-based filtering using the following threshold parameters: nFeature_RNA (3000–9000) and percentage of mitochondrial genes expressed (<15%). For the IPLC dataset, we randomly sampled 1,000 cells for comparison with the stromal subsets of the kidney organoids and HEK. We merged the filtered subset of raw count matrices, performed a SCTransform, v2 regularization[106] standard workflow and chose the percent.mt and cell-cycle scores of genes related to G2/M and S phase[107] as variables to regress out and visualize the expression of the marker genes (Figures 4C, 4D, and Item S2-4D). We annotated cells of the kidney organoids and the downloaded gestational days 96 and 108 HEK tissue dataset using DevKidCC_0.3.0.[48] We performed homology mapping of marker genes of mice to human using Ensembl Archive Release 105 (Dec 2021) and R package biomaRt (Ensembl).

For the downloaded GW14 human embryonic kidney cortex dataset (GEO: GSM4135994 and GEO: GSM4135995; 10x genomics v2 reagent), we used deposited count tables[62] (GRCh37) processed by the Cell Ranger v2.1 pipeline and performed Seurat-based filtering using the following threshold parameters: nFeature_RNA (1000–8000) and the percentage of mitochondrial genes expressed (<10%). For this two-kidney cortex dataset from a single individual,[62] we performed batch correction using the IntegrateData[105] function of Seurat R package v4.0.4 for the initial UMAP representation and clustering to a subset of the data (Figure S6A). However, when using batch uncorrected count data, we annotated the cells using DevKidCC_0.2.3[48] and performed a downstream analysis following a standard NormalizeData, FindVariableFeatures, ScaleData workflow of Seurat.

A pseudo-time trajectory analysis was performed using monocle 2.20.0.[108] DEGs were identified as log2fc > 0.25 using the FindAllMarker function (Seurat) and used for the cluster identification and Metascape analysis. Gene clustering by analyzing

pseudotemporal expression patterns was performed using the differential GeneTest function (monocle2) with a cutoff q value <0.1, and the clustered gene sets were used for the signal pathway analysis with IPA software (Qiagen).

Bulk RNA-seq data processing

For the analysis shown in Figure 1E, transcript quantification was performed using Salmon[109] with the GRCh38.p13 ENSEMBL release 103 cDNA sequence file. The gene definitions were based on GRCh38 GENCODE release 38. The output from Salmon was then processed using the R/Bioconductor package tximport to acquire gene expression values. Gene expressions with fold change values of log2(scaledTPM+1) in IPLCs compared to PPS cells are shown (Figure 1E and Item S5-1E). A heatmap of the gene expressions was generated using the ggplot2_3.3.4 library in R.4.1.0.

For the analysis shown in Figure S3D, gene expression quantification was done using the analysis pipeline (2.3.4) used in the ENCODE project (https://www.encodeproject.org/pipelines/ENCPL002LPE/). GRCh38 ENSEMBL release 104 was used for the reference sequence. Gene definitions were based on GRCh38 GENCODE release 38. The TPM values calculated by the above pipeline (STAR-RSEM) are shown in Item S5-S3D. Genes for which no samples had TPM>1 were excluded from the analysis. Log2(TPM+1) was used for the PCA. We performed a comparative analysis of induced IPLCs treated with or without RA using DESeq2[110] with the expected count calculated by the above pipeline (STAR-RSEM).

For the analysis shown in Figure S7F, transcript quantification was performed using Salmon with the transcript sequences (a concatenated file of GRCh37.p13 cDNA and ncRNA) and the genome sequences as the decoy.[111] The output from Salmon was then processed using tximport to acquire gene expression values. Gene definitions were based on GRCh37 GENCODE release 19 to use a closer genomic annotation of the downloaded GW14 human embryonic kidney scRNA-seq dataset (GEO: GSM4135994 and GEO: GSM4135995). We then performed the comparative analysis using DESeq.[110]

Image quantification of marker Protein(+) cells

Images were captured using an FV3000 confocal microscope and analyzed with the analyze particle function (ImageJ) to calculate the percentage of target protein(+) cells among the total number of Hoechst 33342(+) cells. The protocol for the image analysis was optimized using no primary antibody negative controls.

Statistical analysis

Data are expressed as the mean ± SEM. Student's t-tests were performed to compare mean values when the experimental design was composed of two individual groups. One-way ANOVA and the Tukey-Kramer post hoc test were used for multiple group comparisons in Item S1.